To the Graduate Council:

I am submitting herewith a thesis written by Keith A. Milam entitled "Accuracy of Plagioclase Compositions from Laboratory and Mars Spacecraft Thermal Emission Spectra." I have examined the final paper copy of this thesis for form and content and recommend that it be accepted in partial fulfillment of the requirements for the degree of Master of Science, with a major in Geology.

Harry Y. McSween, Jr., Major Professor

We have read this thesis and
recommend its acceptance:

Lawrence A. Taylor

Jeffrey Moersch

Acceptance for the Council:

Vice Provost and Dean of
Graduate Studies

ACCURACY OF PLAGIOCLASE COMPOSITIONS FROM LABORATORY AND MARS SPACECRAFT THERMAL EMISSION SPECTRA

A Thesis
Presented for the
Master of Science
Degree
The University of Tennessee, Knoxville

Keith A. Milam
August 2002

Dedication

This thesis is dedicated to my wonderful wife Kerry and my son Zacary, who have tolerated my long days and nights in graduate school and have supported me along the way. It is also dedicated my parents, Kenneth and Millie Milam, who have supported me in my scholastic efforts. I want to especially dedicate my thesis to the late Dr. Deborah Kuehn, who inspired me to new heights as an undergraduate geology student and first encouraged me to do my own research.

Acknowledgements

I wish to thank all of those who helped me in completing my Master of Science in the Geological Sciences. I thank Dr. Harry ("Hap") Y. McSween, Jr. for his guidance along the way and help in shaping the mind and abilities of a young scientist. I also thank Dr. Jeffrey Moersch for introducing me to the numerous concepts, problems, and complexities of remote sensing. I appreciate Dr. Larry Taylor for his constructive criticism of my work and writing abilities all along the way. Thanks go to Dr. Victoria Hamilton for getting me excited about Martian remote sensing and wanting to do laboratory verification of remote sensing data.

A million thanks go to Alan Patchen for his untiring assistance while using the electron microprobe. I really appreciate the assistance of Michael Wyatt, who has helped me in deconvolving spectra, in troubleshooting my own thoughts, and showing me what it means to be a good scientist. Terri Geisler (Bureau of Land Management), her husband Don Geisler, Dr. Marvin Beeson (Portland State University), and Julie Donnelly-Nolan (USGS) provided assistance in the field, collecting Columbia River and Steens Basalts. More thanks goes to Dr. Jim Gutmann (Weslyan University) and Molly McCanta (Brown University) for providing samples from the Pinacate Volcanic Field and Black Buttes, CA respectively.

I thank those organizations who have financially supported my graduate research: the National Aeronautics and Space Administration (Mars Data Analysis Program Grant # NAG5-10525), the Mayo Educational Foundation, the Knoxville Gem and Mineral Society, and the Meteoritical Society.

Finally, I thank all of my family and friends, whose encouragement and support has made this work possible.

Abstract

Plagioclase, among the most abundant minerals in terrestrial and martian volcanic rocks, exhibits a range of compositions that reflects changing conditions of lava during crystallization. Average plagioclase compositions of most volcanic rocks are often more sodic than the median of the compositional range, due to the volumetric sub ordinance of calcic plagioclase phenocrysts to more sodic plagioclase in the groundmass. Thermal emission spectrometers (TES, THEMIS, and Mini-TES) onboard Mars spacecraft (Mars Global Surveyor, Mars Odyssey, Mars Exploration Rovers respectively) now provide a means of determining average plagioclase compositions of martian rocks directly.

This study demonstrates that spectrally-modeled average plagioclase compositions in terrestrial basalts, andesites, and dacites correspond approximately to measured values (estimated from the weighted average of electron microprobe analyses of phenocrysts and groundmass grains, and from calculated normative plagioclase compositions). Linear deconvolution of the thermal emission spectra of volcanic rocks can generally model plagioclase compositions to within +10/-6 An (Ca/(Ca+Na)) and +13/-14 An of weighted average and normative plagioclase compositions respectively.

Analyses of spectra from two-component plagioclase sand mixtures (whose plagioclase components varied by volume and composition) have provided additional insight into the role of plagioclase zoning (TES spectra mostly reflect spectral contributions from sand-size particles, which could have been derived by comminution of larger zoned grains). Deconvolutions involving different plagioclase endmember sets produce modeled average plagioclase compositions that closely represent measured values. Considering the variability in types of observed plagioclase zoning patterns in terrestrial volcanic rocks, normal zoning (calcic cores and sodic rims) cannot be assumed and thus does not account for the apparent sodic bias in spectrally modeled compositions. The role of zoning is minimal when compared to the influence of more abundant sodic plagioclase in groundmass. Sand mixture deconvolutions also predict that martian spacecraft TES, THEMIS, and Mini-TES instruments (with variable spatial and spectral resolutions) can model plagioclase compositions to within +3/-8 An, +11/-6 An, and +3/-

8 An (respectively) of measured values in plagioclase mixtures not involving albite. The presence of other phases apparently increases uncertainties, as observed in rock spectra. Nevertheless, this study provides an increased level of confidence in accurately determining plagioclase compositions from Mars thermal emission spectra.

Table of Contents

List of Tables

List of Figures

List of Plates

1. Introduction

1.1 Overview

Remote sensing techniques used in gathering compositional data from planetary surfaces and atmospheres are crucial to understanding planetary geological processes and evolution. From the humble beginnings of telescopic observation to the advanced technologies onboard interplanetary spacecraft, the ability to detect and interpret electromagnetic radiation has proven useful in studies of unsampled solar system bodies. Modern-day remote sensing instruments detect wavelengths of the electromagnetic spectrum beyond that of visible light, ranging from gamma rays (<0.1 Å wavelengths) to radio waves (>100 km wavelengths). When various wavelengths of electromagnetic radiation interact with matter, the resultant spectrum varies as a function of the internal structure and composition of the material. Thus, non-visible wavelengths can be used to identify the materials comprising planetary surfaces and atmospheres. Some wavelength ranges are more suitable for detection of geologic materials than others. For example, Short Wavelength Infrared (SWIR), at 1-3 μm wavelengths, is used in the detection of many clay minerals due to lesser particle size effects at shorter wavelengths and carbonate rocks due to their characteristic SWIR spectral features that aren't masked by atmospheric components in this wavelength range.

Thermal infrared (TIR) wavelengths (3-50 μm) can also be used for determining compositions of atmospheric and surface materials [*Lyon et al.,* 1959; *Lyon,* 1963; *Logan et al.,* 1970]. A material's TIR spectral properties can be directly related to its structural and compositional characteristics [e.g. *Lyon, 1962*]. All objects at temperatures above absolute zero (0 K) consist of atoms with some degree of internal motion. This internal motion produces radiant energy. An object that absorbs all incoming radiation and radiates energy at the maximum possible rate per unit area at each wavelength for a given temperature is referred to as a blackbody. The resulting spectrum follows a Planck distribution. However, most natural materials are not blackbodies. Internal vibrational motions lead to absorption features characteristic of the emitting material. Many common rock-forming minerals have absorption features in the TIR range. Rock-

forming silicates have vibrational motions associated with Si-O stretching modes that lead to characteristic absorption features occurring between 8-12μm, 1250-833 wavenumber, (Figure 1). Carbonates have strong absorption features at 6-8 μm due to CO_3 vibrational motions. Clays show features associated with OH, whereas sulfates and phosphates have absorption features associated with the vibrational motions of SO_4 and PO_4, respectively. Thus, by comparisons of thermal infrared spectra, it is possible to identify and distinguish between minerals, making thermal infrared spectroscopy an invaluable tool for remote sensing of planetary bodies.

1.2 Applications of Infrared Spectroscopy

Infrared spectroscopy has been applied to a wide variety of geological remote-sensing studies on Earth. TIR spectroscopy has typically been utilized for mapping of prominent surface units and thermal features [*Kahle, et al.,* 1997]. TIR spectroscopy has also been applied to: the relative age dating of lava flows [*Kahle et al.*, 1988], mineral exploration [*Watson and Rowan*, 1996], mapping of volcanic thermal features [*Oppenheimer et al.,* 1993], monitoring of underground coal fires [Mansor et al., 1994], and even the prediction of earthquakes [*Zheng et al.*, 1996]. Terrestrial applications and related laboratory investigations have provided a means of technique verification that has allowed geoscientists to apply remote sensing abilities to other planetary environments.

In addition to terrestrial studies, infrared spectroscopy has been used in planetary science applications. Thermal infrared spectroscopy has been used to interpret surface compositions on the Moon and Mercury [*Lucey,* 1991; *Kozlowski*, 1989, *Tyler*, 1988]. Both the Voyager 1 and 2 spacecraft carried Infrared Interferometer Spectrometer and Radiometer instruments [*Livingstone,* 1990] to gather compositional and thermal information from outer solar system planets [*Lunine,* 1989; *Nelson*, 1990]. Currently, the Galileo mission to Jupiter uses the NIMS (Near-Infrared Mapping Spectrometer) to collect infrared spectra from Io to recover temperature and compositional data from Jupiter's most active satellite [*Lopes*, 1997]. The Cassini spacecraft, presently in transit to Saturn, carries two infrared instruments, CIRS (Composite Infrared Spectrometer) and VIMS (Visual and Infrared Mapping Spectrometer), set to determine atmospheric an

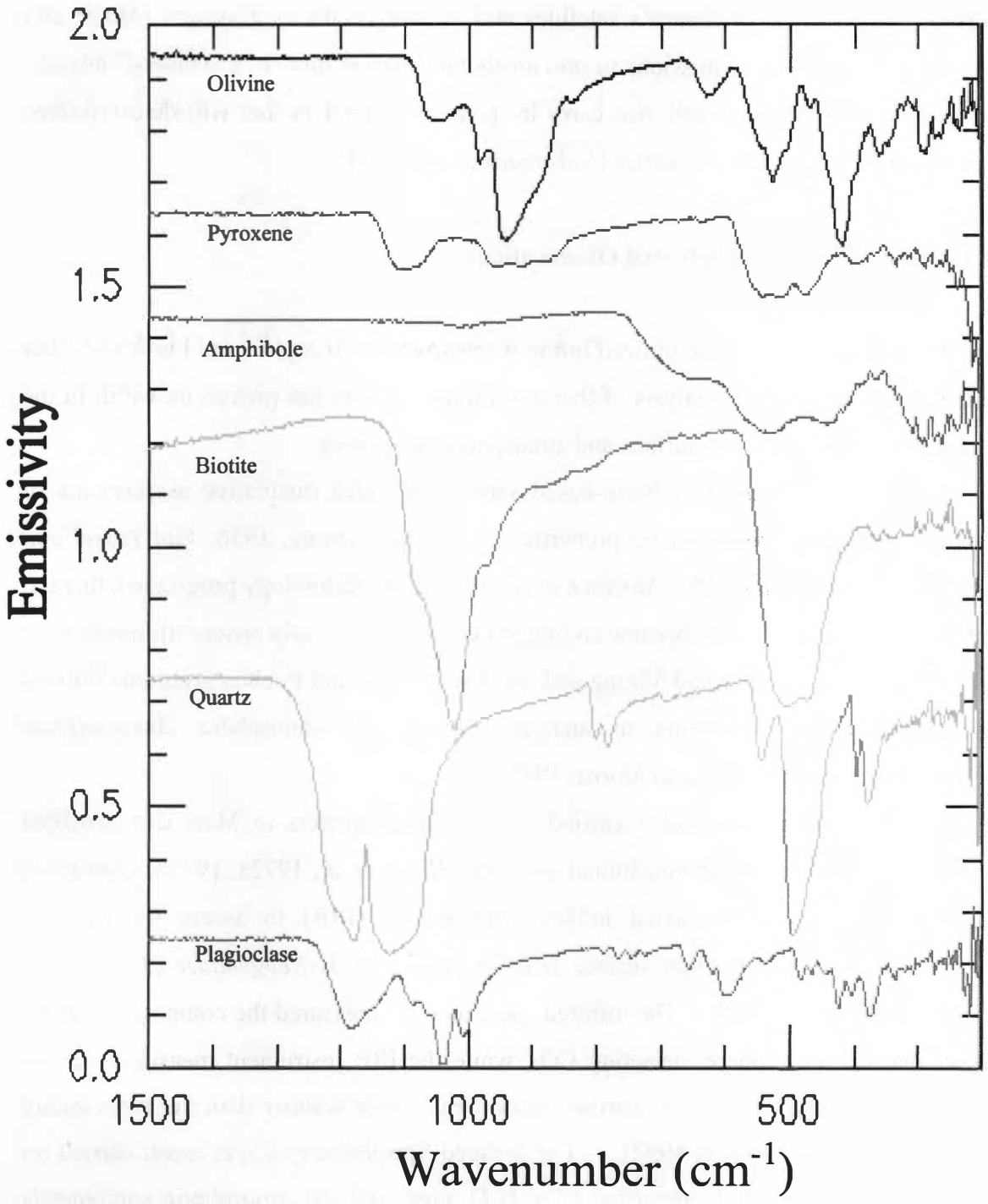

Figure 1. Thermal emissivity spectra of common rock-forming silicates. Emissivity values are offset for clarity. Spectra obtained from the Arizona State University (ASU) spectral library [*Christensen, et al.*, 2000].

surface compositions of Saturn's satellites and to analyze the ring system [*Miner and Gombosi*, 2000]. Future missions to previously unvisited bodies (e. g. Muses-C mission to asteroid 4660 Nereus) will also carry infrared spectrometers that will detect surface mineralogical/geological properties [*Nakamura et al.,* 2001].

1.3. History of Martian Infrared Observations

While geoscientists have utilized infrared spectroscopy to explore the Earth and other solar system bodies, the analysis of thermal infrared spectra has proven its worth in the characterization of martian surface and atmospheric properties.

Early observations from Earth-based sensors provided qualitative assessments of martian surface and atmospheric properties [*Sinton and Strong*, 1956; *Van Tassel and Salisbury*, 1964; *Sinton*, 1967; *Moersch et al.,* 1995]. As technology progressed, thermal infrared spectrometers later became an integral component of early spacecraft missions to Mars. The U.S. Mariner and Viking and the Soviet Mars and Phobos programs utilized thermal infrared instruments to analyze surface and atmosphere characteristics [*Christensen*, 1992; *Snyder and Moroz*, 1992].

In 1969, Mariners 6 and 7 carried infrared spectrometers to Mars that provided surface and atmospheric compositional data sets [*Hanel et al.*, 1972a, 1972b; *Conrath et al.*, 1973]. They also carried infrared radiometers (IRR) to assess the physical characteristics of the martian surface [*Kieffer et al.*, 1973; *Neugebauer et al.,* 1971, *Snyder and Moroz*, 1992]. The infrared spectrometers measured the composition of the lower martian atmosphere, detecting CO_2, while the IRR instrument measured surface temperatures, determining that martian "dark areas" were warmer than the surrounding terrain [*Snyder and Moroz*, 1992]. The Infrared Spectrometry Experiment, carried on board Mariner 9 in 1971, identified CO_2, H_2O, dust, and ice atmospheric components while measuring water vapor and temperature atmospheric properties [*Hanel et al.,* 1972a; *Hanel*, 1973].

Between 1971-1973, three Soviet missions, Mars 2, 3, and 5, each used infrared radiometers (8-40 μm) to investigate martian surface temperatures. These instruments

measured thermal inertia of surfaces consistent with that of dust and determined that dark albedo regions are 10-15^0 degrees warmer than bright areas [*Snyder and Moroz*, 1992]. The infrared radiometer aboard Mars 5 measured surface temperatures between 200-272 K. Thermal inertia data from this instrument allowed for estimates of Martian soil size of between 0.1-0.5 mm [*Ksanfomality & Moroz*, 1975].

In 1976, Vikings 1 and 2 began a new era in Mars exploration. Both missions consisted of an orbiter and a lander. Each of the Viking orbiters carried Infrared Thermal Mappers (IRTM) that were used to measure thermophysical properties (albedo, temperature, and thermal inertia) of the Martian surface and to investigate atmospheric properties [*Kieffer et al.,* 1976]. The Viking IRTM measured thermal emission from the surface in four bands: 6.1-8.3, 8.3-9.8, 9.8-12.5 and 17.7-24 μm. The IRTM instrument measured surface temperatures of between 183-268 K near the Viking landers to as low as 125 K at the martian south pole [*Kieffer*, 1976; *Soffen & Snyder*, 1976]. Polar temperatures were noted to be below the condensation temperature for CO_2, supporting a south pole with carbon dioxide ice [*Kieffer et al.,* 1976a]. Viking-IRTM data also revealed diurnal variations in surface and atmosphere temperatures [*Kieffer et al.,* 1976b].

Thirteen years following the successful Viking program, the USSR sent twin probes to study Mars and one of its moons, Phobos. Despite the failure of Phobos 1, the Phobos 2 spacecraft delivered 4 NIR and TIR infrared instruments (ISM, August, Termoskan, and KRFM) into Mars orbit. One instrument from this group, the French-built ISM-Near Infrared Mapping Spectrometer (0.76-3.14 μm), provided multi-spectral images of Mars that were used for identifying surface mineralogy and atmospheric properties. ISM's spatial resolution varied from 6-30 km/pixel, with a resolving power of ~50, and the instrument collected 128 spectral pixels/spatial pixel [*Bibring et al.,* 1989]. Multi-spectral maps were produced that centered on equatorial and tropical regions. ISM data suggested the presence of hydrated minerals and Fe-rich silicates on a global scale [*Bibring et al.*, 1989]. ISM detected atmospheric dust, CO, CO_2 and H_2O and measured each component's spatial variability across Mars [*Combes et al.,* 1991]. Variations in the CO_2 2 μm absorption band were also used to extrapolate surface altitude information [*Bibring et al.*, 1991].

1.4. Current TIR Investigations of Mars

Mars exploration continues to involve use of thermal infrared sensors. NASA's Mars Global Surveyor (MGS), currently in a 350 km martian orbit, uses the Thermal Emission Spectrometer (TES) [*Christensen et al.*, 1992; *Christensen et al.*, 2001a] to determine rock types and modal mineralogies of surface lithologies [*Bandfield et al.*, 2000a; *Hamilton and Christensen*, 2000; *Hamilton et al.*, 2000, *Christensen*, 2001]. TES is a Fourier transform Michelson interferometer that collects spectra over the 5.8-50 μm wavelength (1709-200 cm^{-1} wavenumber) range with 5 and 10 cm^{-1} spectral and 3x5 km spatial resolution. During its initial mapping phase, which lasted approximately one martian year, the TES instrument collected approximately $5x10^7$ million spectra.

TES spectra are calibrated to radiance by collecting reference spectra from space and an internal reference surface. Radiance values are then converted to emissivity (ε) by dividing radiance by the Planck function at the kinetic temperature of the surface [*Christensen et al.*, 2001a]. Kinetic surface temperatures are derived as described by *Christensen et al.* [2001b]. Emissivity spectra are favored over radiance because changes in temperature lead to changes in radiance. In order to compare spectra of materials emitting at different temperatures, this temperature effect must be removed. After removing temperature effects, emissivity spectra still contain atmospheric dust, CO_2, and H_2O contributions that can then be removed by methods described by *Bandfield et al.*, [2000b] and *Smith et al.*, [2000]. The remaining spectra contain compositional and abundance information for martian surface materials.

To extract compositional information from martian surface spectra, a linear deconvolution technique [*Ramsey and Christensen*, 1998] is then applied. Linear deconvolution is based on the principle that spectral radiance from isothermal minerals in rocks and particulate mixtures combine linearly in proportion to their areal percentages to produce a composite spectrum. This spectrum can then be "unmixed" to reveal modal and compositional mineral information. The linear deconvolution algorithm requires an input spectrum, a library of pure spectral endmembers, and the wavenumber range over which the spectrum is to be deconvolved (Figure 2). The algorithm performs a linear

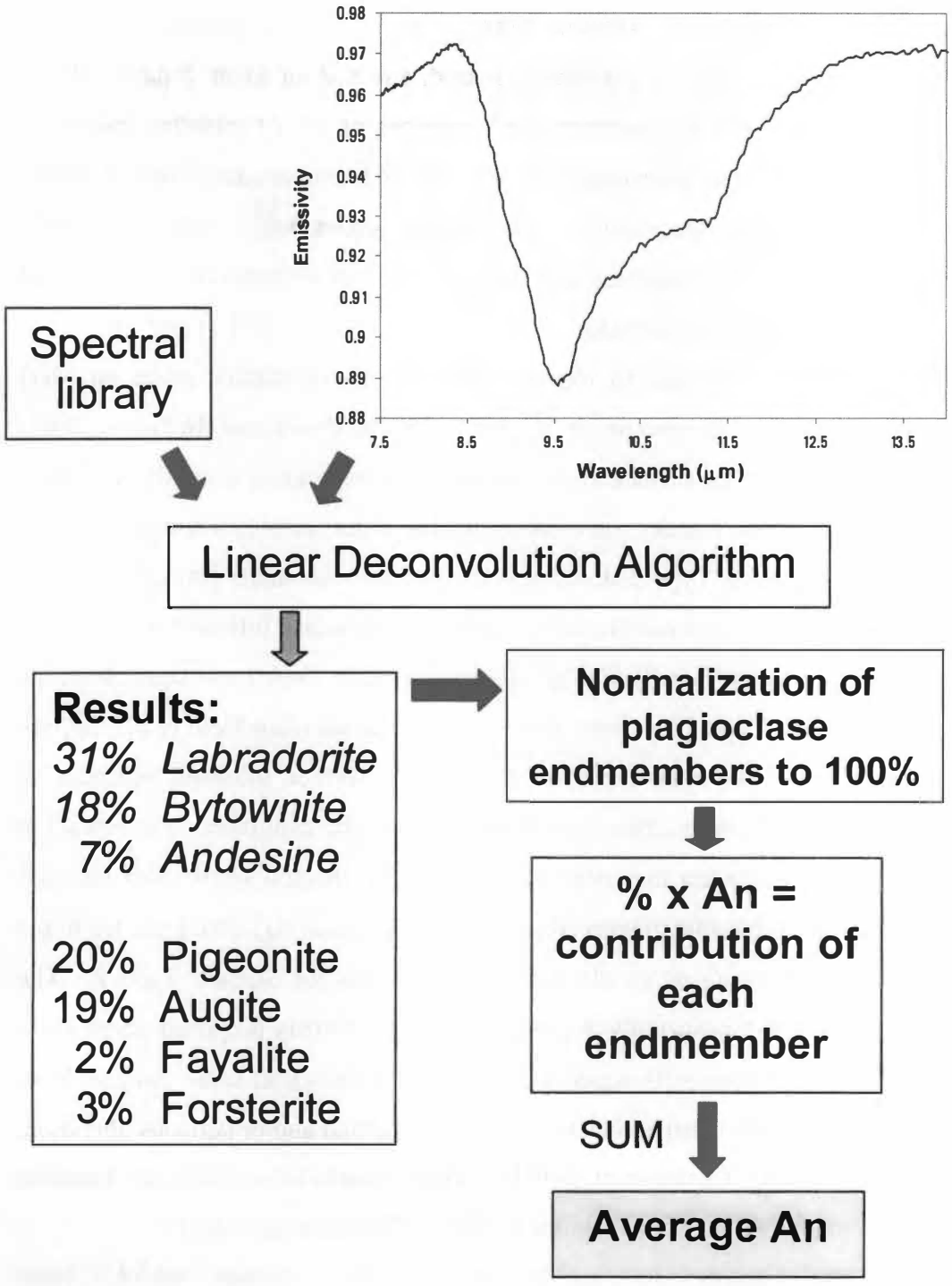

Figure 2. Flow chart showing how plagioclase composition is determined from a basalt rock spectrum. The spectrum is first deconvolved using a spectral endmember library. Volume percentages of spectral endmembers used are then normalized, multiplied by their respective measured An's, and added together to estimate the average plagioclase composition for the rock.

least-squares fit to the spectrum. Outputs from the deconvolution include a "best fit" modeled spectrum, percentages of endmembers used, and a Root Mean Squared (RMS error. RMS errors are used to determine the "goodness of fit" of modeled spectra to measured spectra. Reported percentages of spectral endmembers used reflect modal mineralogies for measured specimens. Pure spectral endmembers have been well-characterized by geochemical analyses and thus, are used to extrapolate compositional information about remotely sensed rocks.

TES data have been used to identify three prominent surface types on Mars [*Bandfield et al.,* 2000a; *Christensen, et al.*, 2001; 2001b; *Wyatt and McSween*, 2001; 2002]. Two of the martian surface types are spatially associated with the planetary dichotomy. Surface Type 1 rocks are common in the older, heavily cratered southern highlands, whereas Surface Type 2 dominates the northern lowlands [*Bandfield et al.*, 2000a]. Both surface types are dominated globally by plagioclase followed by pyroxene and glass in lesser amounts [*Bandfield et al.*, 2000a]. Surface Type 1 has been identified as basalt while Surface Type 2 has been identified as andesite [*Bandfield et al.*, 2000a]. The presence of these two rock types on the martian surface indicates episodes of extensive volcanic activity with differing amounts of magmatic evolution. A recent set of deconvolutions of TES spectra that take into account the spectral similarities between andesitic and weathered basaltic glasses [*Wyatt and McSween*, 2001; 2002] has led to the proposal of weathered basalt as an alternative composition for Surface Type 2. The proposed weathered basalt is spatially associated with a previously proposed ocean basin [*Head et al.,* 1999] consistent with aqueous alteration of minerals at some point in Mars history. Hematite deposits, often associated with hydrothermal and/or aqueous alteration, have also been identified [*Christensen,* 2001b]. These equatorial deposits are found in the Sinus Meridiani and Aram Chaos regions on Mars [*Christensen*, 2001b].

The Thermal Emission Imaging System (THEMIS), onboard NASA's Mars Odyssey orbiter, uses thermal infrared technology to detect surface and atmospheric thermophysical and compositional properties. THEMIS [*Christensen et al., 2002*] has higher spatial (100 meters/pixel) and much lower spectral resolutions than the MGS-TES instrument. THEMIS collects spectra over 10 spectral bands from 6.5-14.5μm (1540-690

cm^{-1}). It acquires visible images over 5 visible wavelength bands with 20 meters/pixel spatial resolution. This instrument is designed to search for small-scale mineral deposits that may be associated with areas of hydrothermal or sub-aqueous alteration. The instrument also looks for subsurface thermal anomalies and is presently characterizing potential landing sites for the 2003 Mars Exploration Rover (MER) missions.

NASA's two MERs are set to arrive on the surface of Mars in early 2004, each carrying Miniature Thermal Emission Spectrometer (Mini-TES) instruments [*Christensen et al.*, 2000]. Each Mini-TES will collect surface spectra between 5-29 μm (2000-345 cm^{-1}) with high spatial resolution at their respective landing sites. Spectra will be collected over short (cms) and long (km) pathlengths. To avoid collecting spectra from dust-covered surfaces, each MER rover will carry a Rover Abrasion Tool (RAT), which will remove dust and weathering rinds to reveal fresh rock surfaces. The RAT will remove dust and weathered material from an area ~4.5 cm in diameter and will penetrate 5 mm in depth. Following dust removal, the rover rolls back and aims a panoramic imager (Pancam) at the fresh surface for multiband image collection. Each Mini-TES instrument will be housed within the rover body and will work with Pancam to collect spectral images in 360^0 and $+30^0$ to -50^0 from the horizontal.

The European Space Agency (ESA) also has its own plans for utilizing infrared spectroscopy in martian studies. ESA plans to launch the Mars Express mission in 2003, carrying the Omega IR mapping spectrometer whose purpose is mapping the mineral composition of the martian surface and analyzing martian atmospheric components [*Bibring*, 2000]. Omega will utilize two channels, 0.5-1.0 μm for visible wavelengths and 1.0-5.2 μm for the infrared.

With such a fleet carrying infrared spectrometers to the Red Planet, the importance of IR spectroscopy to martian remote sensing studies is clear. Current and previous spectral studies of Mars using thermal emission data have provided a great deal of insight into martian geologic processes. While VisNIR spectroscopy has the ability to detect ferromagnesian minerals, thermal infrared wavelengths have provided a great deal of information about silicate minerals on Mars.

For the first time, deconvolutions of TES spectra have allowed geologists to analyze the mineralogy of martian surface types [*Bandfield et al.,* 2000a; *Hamilton et al.,* 2001a; *Wyatt & McSween*, 2002]. Deconvolution results indicate that both surface types are dominated by plagioclase, followed by lesser amounts of clinopyroxene (Surface Type 1) and volcanic glass (Surface Type 2). Such mineralogy is common in terrestrial basalts and andesites. Plagioclase in terrestrial rocks occurs as a solid solution series mineral, ranging from the more Ca-rich variety, anorthite ($CaAl_2Si_2O_8$), to the Na-rich variety, albite ($NaAlSi_3O_8$), with a variety of intermediate compositions. Compositional variability, due to coupled substitutions between Ca-Na and Al-Si, results from changing P-T conditions during fractional crystallization. Typically, at higher temperatures, the Ca-rich varieties of plagioclase are first to crystallize, followed by increasingly more sodic plagioclase. Variable, non-equilibrium conditions during crystallization also leads to zoning in plagioclase. Zoning patterns include: normal (Ca-rich core to Na-rich rim), reverse (Na-rich core to Ca-rich rim), oscillatory, and multiple combinations of these. Most plagioclase in unaltered terrestrial basalts and andesites are intermediate to calcic in composition, rarely $<An_{30}$. Basalts and andesites with plagioclase compositions $<An_{30}$ have commonly experienced some form of metasomatic, hydrothermal, or subaqueous alteration. Continued alteration/weathering of plagioclase results in a variety of clay minerals. Thus, extensive petrologic study of plagioclase and precise determination of its composition provides insight into magmatic P-T conditions and subaqueous alteration/weathering of rock. With deconvolutions of thermal emission spectra identifying plagioclase as a primary mineral in the martian crust, our ability to determine plagioclase abundances and compositions is also important to understanding martian geologic processes. While previous studies [*Wyatt et al.*, 2001] have shown the precision with which plagioclase abundances can be estimated, determination of plagioclase compositions from thermal emission spectra is even more challenging and requires extensive laboratory verification. However, in this case as in many others, laboratory verification and comparisons to terrestrial analogs often lag behind the interpretation of remote sensing data.

2. Purpose of This Study

In a study of the application of thermal emission spectra to the classification of terrestrial and martian volcanic rock compositions, *Wyatt et al.*,[2001] deconvolved mineral abundances for volcanic rocks ranging in composition from basalt to dacite. Plagioclase compositions were modeled (Figure 2) by normalizing percentages of the total plagioclase endmembers used in the deconvolution to 100%, multiplying individual contributions by their respective anorthite contents (An's), and summing the results. Anorthite content, the molar ratio of Ca/Ca+Na in solid solution plagioclase, has been determined in library standards from laboratory measurements [*Christensen et al.*, 2000 and augmented by measurements from this study]. Modeled An (anorthite content x 100) was then compared to measured plagioclase compositional ranges for each sample (Figure 3). In the 18 rocks studied, 14 modeled compositions were within reported plagioclase compositional ranges for each sample. However, these 14 modeled compositions were all more sodic (i.e. Na-rich, higher albite ($NaAlSi_3O_8$) component) than median values for the measured compositional ranges. The remaining 4 modeled compositions were more sodic and outside measured compositional ranges. Results suggested an apparent "sodic bias", introducing the possibility of non-linear mixing in complex mixtures of plagioclase having variable compositions. Plagioclase compositional variability is ubiquitous in volcanic rocks due to changes in the P-T conditions of a crystallizing melt. Inability to accurately determine plagioclase compositions would limit interpretations of martian petrogenetic processes.

Wyatt et al. [2001] hypothesized that the sodic trend in modeled plagioclase compositions resulted from the fact that TIR-derived plagioclase compositions represent an average of all plagioclase in a given sample. They suggested that the "sodic bias" resulted from the volumetrically dominant contributions of more sodic groundmass and more sodic rim material on large normally zoned phenocrysts to the overall rock spectra.

This study examines both parts of the *Wyatt et al.* [2001] hypothesis. Part I focuses on the role of plagioclase phenocryst and groundmass mixing. Part I examines

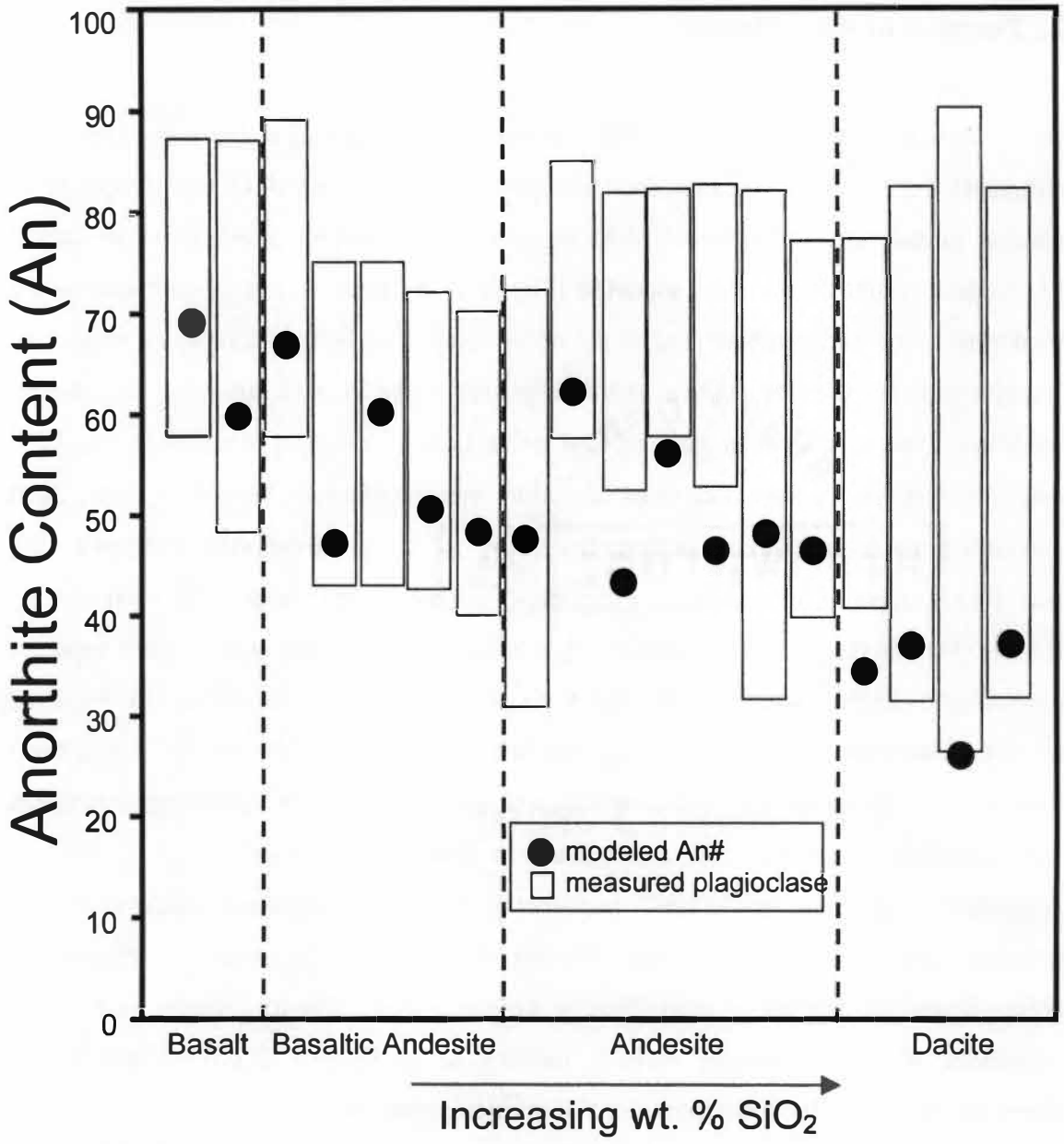

Figure 3. Comparison of modeled plagioclase compositions with measured plagioclase compositional ranges, modified from *Wyatt et al.* [2001]. Note modeled values plot near the Na-rich ends of measured compositional ranges. Four modeled values lie outside measured plagioclase compositional ranges.

laboratory geochemical and spectral analyses of terrestrial volcanic rocks to address the following questions:

(1) Are the assumptions of sodic plagioclase in mesostasis and normal zoning as the dominant plagioclase zoning pattern in terrestrial volcanic rocks correct?

(2) Were the reported plagioclase compositions of *Wyatt et al.*, [2001] representative of actual compositional ranges?

(3) Is the apparent "sodic bias" influenced by the linear mixing of a volumetrically more dominant sodic groundmass with typically more calcic phenocrysts?

Part II assesses the potential effects of plagioclase zoning on thermal emission spectra of volcanic rocks. Sand mixtures are used to provide compositional and volumetric control over simulated plagioclase "zoning" and are thought to represent plagioclase comminuted by physical weathering processes. Geochemical and spectral analyses of plagioclase sand mixed in variable proportions and over different compositional ranges were performed to provide insight into the following questions:

(1) Can spectra of simulated zoned plagioclase be accurately represented as a linear mixture of individual zone spectra? OR

(2) Does simulated plagioclase zoning influence the "sodic bias"?

The results from Parts I and II are then applied to the analysis of TES, THEMIS, and Mini-TES data.

3. Methods

3.1. Part I. Rocks: Phenocrysts vs. Groundmass

3.1.1. Sample Acquisition and Preparation. Volcanic rocks, ranging from basalt to dacite (Figure 4), were selected from a variety of tectonic settings (Table 1). Most specimens (except 79-35i) contained plagioclase as both phenocrysts and groundmass (Figure 5). Several of these samples were acquired by the author (LGF700D, LGF700C, MVO-A, BB-DR, 2524a), while the remainder came from *Kinzler et al.*, [2000] (83-35 and 83-22, courtesy of T. L. Grove) or the more sodic modeled compositions from *Wyatt et al.*, [2001] (79-35i, 79-3b, 79-39d, HK-1, HK-3, and HK-5). Rocks were divided into three portions for various analyses. Thin sections (30 μm thick) of each rock specimen were prepared for petrographic and electron microprobe analysis. Then, 6 g of each sample were ground into clay-sized particles for XRF analysis, while 3 cm-diameter circular rock slabs were cut for spectral analysis.

3.1.2. Petrography. Optical examination was used for preliminary mineral identification. All samples, except 79-35i, have porphyritic textures with variable amounts of euhedral to subhedral plagioclase, pyroxene, olivine, and amphibole phenocrysts. Dacites contain potassium feldspar, amphibole, and quartz phenocrysts. Plagioclase and pyroxene phenocrysts commonly display strong and weak zoning patterns. Most groundmass was too fine-grained to determine compositional heterogeneity. Mesostasis is commonly composed of smaller grains of the phenocryst minerals plus abundant glass and oxide phases. Magnetite, ilmenite, and minor (<2%) amounts of rutile are present. Detailed petrographic descriptions of individual rocks are provided in Appendix A.

3.1.3. Geochemistry. Bulk rock chemistries for rock samples were determined by using X-ray fluorescence (XRF) (Table 1) by ActLabs laboratories in Tuscon, Arizona. A 0.5 gram portion of roasted sample was fused with 6.5 grams of flux composed of 49.75% lithium metaborate, 49.75% lithium tetraborate, and 0.5% lithium bromide. Samples were fused in Pt95%-Au5% crucibles using an automated fluxer and were molded into glass buttons. Glasses were analyzed on a Philips PW 2400

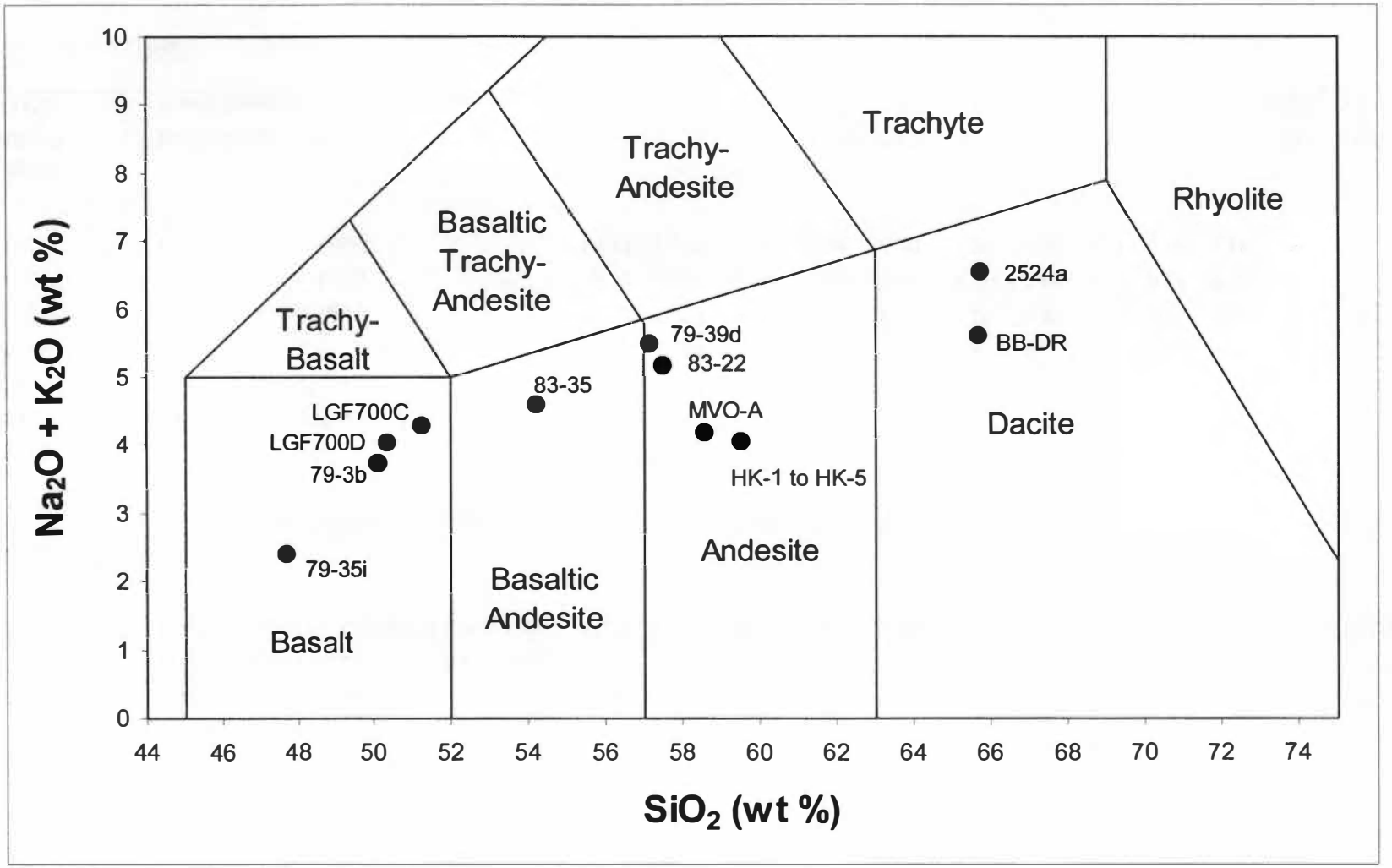

Figure 4. Volcanic rock classification for samples used in Part I. Bulk rock geochemical data for samples 83-35 and 83-22 are from [*Kinzler et al.*, 2000] and samples 79-35i, 79-3b, 79-39d, HK-1, HK-3, and HK-5 from [*Wyatt et al.*, 2001].

Table 1. Sample sources and bulk chemistry for rocks in Part I.

Sample #	Ref.	Locality	SiO_2	Al_2O_3	Fe_2O_3	MgO	CaO	Na_2O	K_2O	TiO_2	P_2O_5	MnO	LOI	TOTAL
Basalts														
79-35i	1,2	Medicine Lake Highlands, CA	47.68	17.74	9.72	9.35	11.74	2.30	0.09	0.71	0.06	0.16		99.55
79-3b	1,2	Medicine Lake Highlands, CA	50.11	20.86	9.10	10.54	3.27	0.47	1.10	0.18	0.13	4.06		99.82
LGF700D	3	Lower Gingko Fm., Col. River Basalt Grp.	50.37	13.40	14.80	3.69	8.54	2.86	1.17	3.35	0.77	0.21	0.85	100.01
LGF700C	3	Lower Gingko Fm., Col. River Basalt Grp.	51.23	13.73	14.29	3.46	8.40	2.85	1.43	3.33	0.68	0.20	0.40	100.00
Basaltic Andesites														
83--35	1	Callahan Flows, Medicine Lake, CA	54.20	17.60	7.65	5.88	8.82	3.66	0.95	0.95	0.17	0.13		100.01
Andesites														
83-22	1	Callahan Flows, Medicine Lake, CA	57.50	17.10	6.75	4.82	7.53	3.70	1.48	0.85	0.16	0.12		100.01
79-39d	1,2	Medicine Lake Highlands, CA	57.15	16.03	7.53	4.29	7.27	3.33	1.82	1.17	0.52	0.11		99.22
MVO-A	3	Montserrat Volcano, Martinique	58.56	17.19	7.39	2.95	7.60	3.37	0.82	0.61	0.15	0.18	0.12	98.94
HK-1	1,2	Hakone volcano, Japan	59.52	16.79	8.64	2.14	6.20	3.21	0.86	1.01	0.15	0.16		98.52
HK-3	1,2	Hakone volcano, Japan	59.52	16.79	8.64	2.14	6.20	3.21	0.86	1.01	0.15	0.16		98.52
HK-5	1,2	Hakone volcano, Japan	59.52	16.79	8.64	2.14	6.20	3.21	0.86	1.01	0.15	0.16		98.52
Dacites														
BB-DR	3	Black Butte, California	65.68	17.23	3.36	1.93	5.07	4.44	1.18	0.41	0.11	0.05	0.52	99.99
2524	3	Dacite Porphyry, Helena, Montana	65.70	15.12	2.94	2.16	3.78	3.75	2.82	0.41	0.13	0.05	3.38	100.25

1= Kinzler et al., [2000] 2= Wyatt et al., [2001] 3= this study

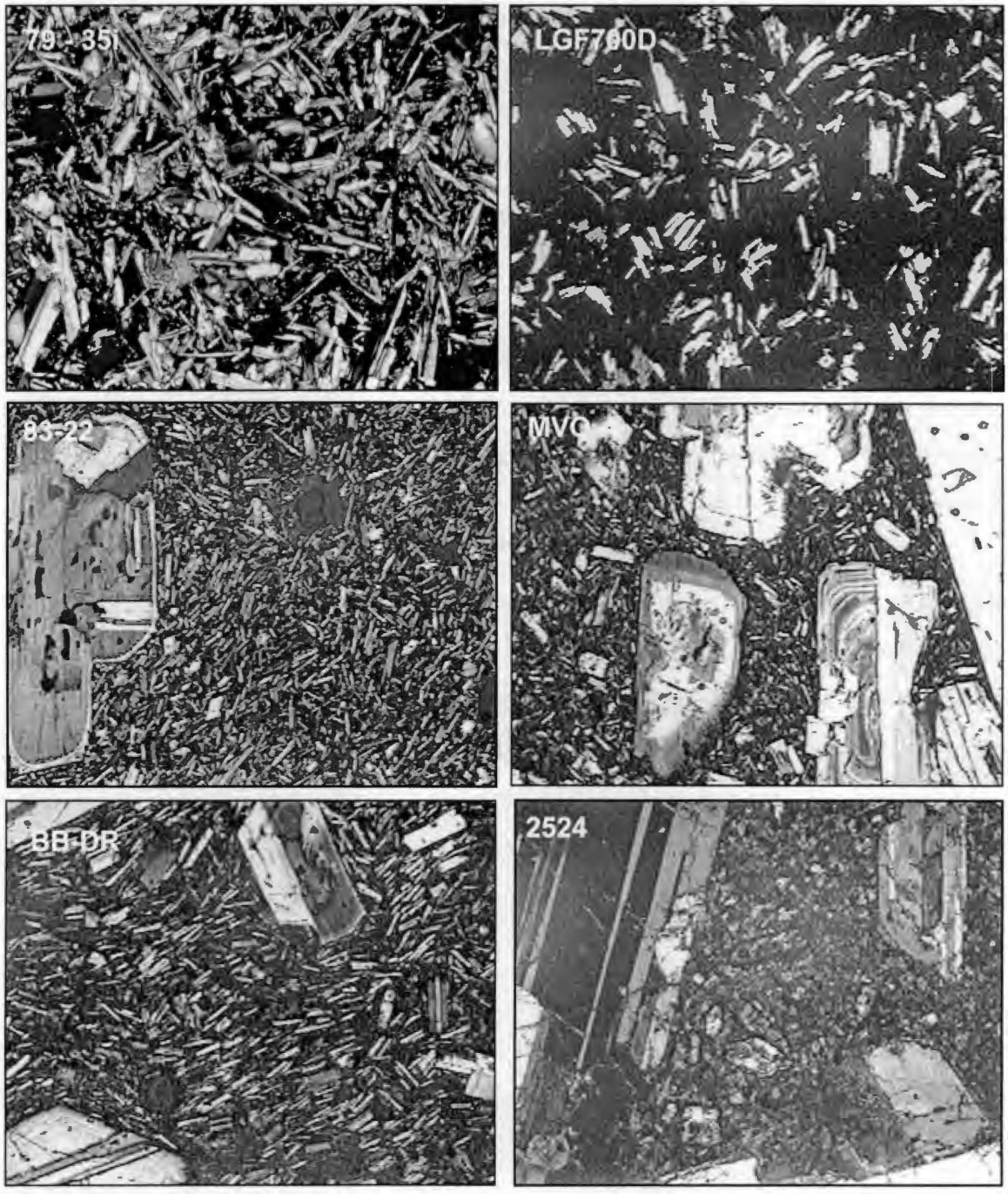

Figure 5. Photomicrographs of representative samples used in Part I. Samples include basalts, basaltic andesites, andesites, and dacites. All samples but 79-35i have porphyritic textures with plagioclase phenocrysts. Note zoning in samples 83-22, MVO-A, BB-DR, and 2524. Photomicrograph widths are 1.78 mm.

sequential wavelength dispersive spectrometer equipped with a 102 position PW2510/26 automatic sample changer. The spectrometer is equipped with a Rh end window X-ray tube, 5 filters, 5 analyzing crystals, and 3 detectors. Data were analyzed on line with Philips proprietary SuperQ software. Control certified reference materials were analyzed along with every batch of samples. Prior to fusion, the loss on ignition (LOI), which includes H_2O+, CO_2, S, and other volatiles, were determined from the weight loss after roasting the sample at 1000^0 C for 2 hours. (The previous description was provided by ActLabs). More detailed XRF sample preparation and analysis techniques are outlined in *Norrish and Hutton*, [1969]. Normative mineralogies were calculated from XRF analysis (Appendix B). Anorthite contents (An) from CIPW-NORM calculations are reported in Table 2.

Chemical analyses using a CAMECA SX-50 electron microprobe determined plagioclase compositions and the presence of zoning by use of core-to-rim transects equally spaced across individual plagioclase phenocrysts and groundmass (Appendix C). Analyses used an accelerating voltage of 15 kV, beam current of 20 nA, and counting times of 20 s per element. Beam size varied, depending on grain size and width of compositional zoning. A 5 or 10-μm size beam was used for coarsely zoned plagioclase phenocrysts, whereas 1, 2, or 5-μm-sized beams were used for plagioclase in mesostasis (typically <20μm diameter). ZAF (Z=atomic #, Absorption, Fluorescence) corrections were applied to all analyses.

Modal mineralogy for each rock was determined by Energy Dispersive Spectrometer (EDS) analyses using the Feature Scan technique [*Taylor et al.*, 1996]. EDS analyses were performed in 8-15 μm steps (depending on the size of the sample area chosen) over grid areas representative of the entire sample. Classification of phases is dependent upon percent contributions of elements to the spectrum from each EDS analysis. Classification schemes are shown in Appendix D. This procedure typically yielded 150,000 analyses per sample. Percentages of unclassified phases varied from 5-17 %, dependent upon grain size of mesostasis. Some of the finest groundmass had grains with dimensions of 1x2 μm, so that many grain boundaries were sampled, leading to a relatively higher percentage of unclassified phases. Based on observations of

backscattered electron (BSE) images, we assume that phases in the fine-grained unclassified mesostasis have the same abundances as the larger measured phases.

Weighted average plagioclase compositions for each sample were calculated from microprobe analyses (Table 2) for comparison with modeled compositions. Feature Scan analyses were used to determine total plagioclase abundance for each sample and point counting (Table 3) with an optical microscope (2000 cts/sample, 290μm step size) was used to determine the plagioclase phenocryst abundance for each sample. The plagioclase groundmass abundance was determined by taking the difference between total and phenocryst plagioclase abundances. Weighted average plagioclase compositions were then calculated by inputting relative abundances and averaged compositions for each of the grain types (phenocryst and groundmass) within each sample.

3.1.4. Spectral Analyses and Deconvolutions. Rock slabs were used for spectral analysis. Polishing results in spectra with deeper and sharper absorption bands as compared to spectra of irregular, weathered surfaces. Samples were heated until a sample temperature of 80^0C was reached and maintained throughout the experiment by a thermostatically-controlled heating element. Spectra were collected using 180 scans of a Nicolet Nexus 670 spectrometer at Arizona State University over 2000-200 cm^{-1} wavenumbers (2.5-50 μm wavelength). Sample radiance was then converted to emissivity using a technique described in *Ruff et al.* [1997].

Rock spectra were "unmixed" using the linear deconvolution algorithm described earlier [*Ramsey and Christensen*, 1998]. This unmixing is based on the assumption that a rock spectrum is a linear mixture of its constituent mineral spectra in proportion to the areal exposure of minerals. Deconvolutions of rock spectra for this part of the study were performed at laboratory resolution using the endmember set from *Wyatt et al.* [2001] (Table 4). This endmember set includes 8 homogeneous plagioclases (Table 5) ranging from An_8 to An_{92}. Rock spectra were deconvolved over the 1280-400 cm^{-1} wavenumber range, which encompasses all of the major silicate absorption bands in the thermal infrared. The algorithm produces modeled spectra (Appendix E) and reports percentages of spectral endmembers used in the deconvolution to model a "best fit" spectrum to that

Table 2. Spectrally modeled, NORM-calculated, and microprobe weighted avg. An's for plagioclase in rocks of Part I.

Sample ID	Modeled An	NORM-calculated An	Weighted Avg. An
79-35i	74.2	64.6	74.2
79-3b	64.0	58.2	65.0
LGF700D	69.0	44.2	48.5
LGF700C	57.0	44.4	56.5
83-35	49.4	46.7	55.2
79-39d	69.2	44.0	59.2
83-22	56.8	43.6	60.3
MVO-A	50.0	49.3	51.9
HK-1	50.6	50.1	52.8
HK-3	56.5	50.1	59.3
HK-5	58.6	50.1	60.9
BB-DR	32.7	37.2	49.3
2524a	18.3	32.3	13.8

Table 3. Data and calculations for weighted average plagioclase compositions in Part I.

	For total rock			For total rock			Of Total Plagioclase					
Sample	**% gm***	**% plag ph.***	**% other ph.***	**% total plag.****	**- % plag ph.***	**% plag gm**	**% plag ph.**	**% plag gm**	**An_{gmavg}*****	**An_{megavg}*****	**1,2**	**An_{avg}**
79-35i	100	0	0	100	0	100	100.0	0	74.2	0		74.2
79-3b	92.4	5.4	1.7	46	5.4	40.6	88.3	11.7	55.0	80.1		65.0
LGF700D	97.1	2.35	0.55	33.93	2.35	31.58	93.1	6.9	47.8	57.6		48.5
LGF700C	95.68	1.3	0	49.12	1.3	47.82	97.0	3.0	43.1	56.8		43.5
83-35	99.7	0.3	0.05			-0.3	99.0	1.0	55.3	42.4		55.2
79-39d	92.9	5.4	1.7	46	5.4	40.6	40.0	60.0	59.6	56.0		59.2
83-22	93.65	4.4	0.1	51.16	4.4	46.76	91.4	8.6	60.7	56.1		60.3
MVO-A	61.7	26.5	11.8	49.32	26.5	22.82	46.3	53.7	45.1	57.6		51.9
HK-1	81.7	14	4.3	53	14	39	73.6	26.4	47.0	68.8		52.8
HK-3	59.75	30.7	9.55	56	30.7	25.3	45.2	54.8	54.8	63.0		59.3
HK-5	50	31.95	18.05	53	31.95	21.05	39.7	60.3	39.7	64.1		60.9
BB-DR	89.2	7.5	3.2	49.43	7.5	41.93	84.8	15.2	47.0	62.4		49.3
2524a	58.5	29.55	12	37.63	29.55	8.08	21.5	78.5	13.8	30.5		13.8

* = from point counting ** = Feature Scan analyses ***= electron microprobe analyses

gm = groundmass ph = phenocryst

1 = %plag mega.(x) = (% plag gmass)((Angmegavg-Angmavg)-x)

2 = Anavg =IAnmegavg-xI

Table 4. Bulk chemistries of all plagioclase endmembers used in study. * = indicates [*Wyatt et al.*, 2001] endmember set **=samples selected for this study

Sample I.D.	Source	SiO2	Al2O3	FeO (Fe2O3)	MnO	MgO	CaO	Na2O	K2O	Total	An#
WAR-0235	ASU	68.3	20	0.33	0.01	0.04	0.01	11.5	0.02	100	<1
WAR-0244	ASU	69.2	18.2	0.24	0.01	0.01	0.38	10.2	0.66	98.9	2
WAR-0612	ASU	67.2	19	0	0.02	0.4	0.35	9.26	0.18	96.4	2
5851*	UT	67.9	19.9	0	0.02	0.02	0.63	9.71	0.27	98.5	2
WAR-5851**	ASU	63	19.7	5.51	0.02	0.47	1.37	8.5	0.22	98.8	8
BUR-060D	ASU	63.5	22.5	0.21	0.01	0.01	3.36	9.21	0.6	99.4	15
BUR-060	ASU	60.4	21.9	4.16	0.08	0.06	3.24	9.37	0.79	100	16
WAR-5804**	ASU	62	24	0.04	0	0	4.74	9.03	0.5	100	22
WAR-3680	ASU	63.5	22.7	0.03	0.13	0.44	4.94	7.76	0.63	100	25
WAR-0234	ASU	60.8	22.1	0	0.02	0.85	5.37	6.71	0.91	96.8	29
BUR-240**	ASU	53.9	27.1	0.53	0.01	0.07	9.51	5.55	0.34	97	48
WAR-3080A	ASU	53.4	26.3	1.5	0.03	0.65	9.62	4.94	1.2	97.6	48
WAR-0024	ASU	56.4	24.6	0.06	0.07	2.51	9.38	4.67	0.76	98.5	50
4512A-L*	UT	54.2	24.4	2.16	0.05	1.32	9.8	4.34	1.3	97.6	51
0022b*	UT	54.8	26.5	1.1	0.03	0.24	10.4	4.02	0.47	97.6	53
WAR-4524**	ASU	52.6	27.7	2.5	0.02	0.14	10.9	5.01	0.42	99.3	53
WAR-1384	ASU	51.3	30.9	0.32	0.03	0.5	11.8	3.64	0.26	98.8	63
WAR-RGAND01**	ASU	49.9	28	3.09	0.03	0.68	13	3.46	0.22	98.4	67
SS*	UT	50.9	29.8	0.3	0.02	0.15	13.4	3.42	0.14	98.1	68
WAR-5859**	ASU	48.4	31.5	1.56	0.01	0.26	14.7	2.89	0.09	99.4	73
1382a	UT	49.1	30.4	0.5	0.04	0.45	14.5	2.86	0.2	98.1	73
WAR-5759**	ASU	41.5	29.5	9.2	0.03	2.69	15.4	1.13	0.08	99.5	88
BUR-340**	ASU	43.2	35.6	0.54	0.01	0.39	17.6	0.84	0.01	98.2	92

of the rock spectrum. These percentages reflect mineral abundances in the rock within certain margins of error for each mineral present.

3.2 Part II. Plagioclase Zoning

3.2.1. Sample Acquisition. Initially, samples of large plagioclase were collected from: the Upper and Lower Gingko Flows of the Columbia River Basalt Group near the Willamette River in Portland, Oregon, the Steens River Basalts along the western flank of Steens Mountain, Harney County, Oregon, and the Sunstone Public Collecting Area in Lake County, Oregon. J. T. Gutmann (Wesleyan University) provided large plagioclase phenocrysts from the Pinacate Volcanic Field, Mexico. Phenocrysts were chosen because of their relative ease of extraction from bulk rock samples and the ability to collect large amounts of them. Other samples used in this study were purchased from Ward's Scientific Supply Co.

3.2.2. Sample Selection. Five samples (Table 4) were chosen that ranged from An_2 to An_{73} (filled circles in Figure 6). Specimens were characterized using the optical microscope and electron microprobe to determine the appropriateness (lack of compositional heterogeneity) of their use in this study (Figure 7). Samples showing signs of weathering/alteration or having relatively high percentages (<5%) of impurities were excluded. Also, any plagioclase that displayed optical or compositional zoning patterns were excluded. Plagioclase compositional information was obtained by geochemical analysis using an electron microprobe. Portions of each plagioclase were ground into silt/clay-sized particles and placed on molybdenum strips. Each molybdenum strip holding the sample was placed between two electrodes, whose current was slowly increased, thus increasing the temperature of the metal strip to above the liquidus of plagioclase between 1100^0C-1550^0C. Following complete melting, the electric current was removed to allow the plagioclase melt to be quenched into glass. Twenty-four electron microprobe analyses measured plagioclase compositions for each fused bead (Appendix F). Plagioclase that demonstrated compositional variability more than 5 An were excluded from use in this study.

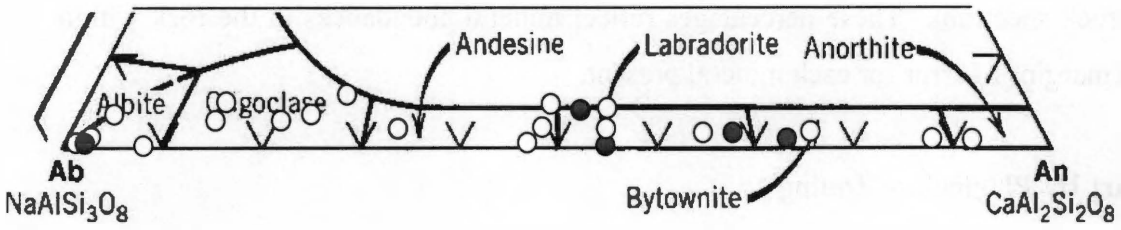

Figure 6. Part II: Plagioclase ternary diagram showing plagioclase compositions for homogeneous plagioclase minerals used in physical mixtures (black circles) and spectral endmembers from the ASU spectral library (open circles).

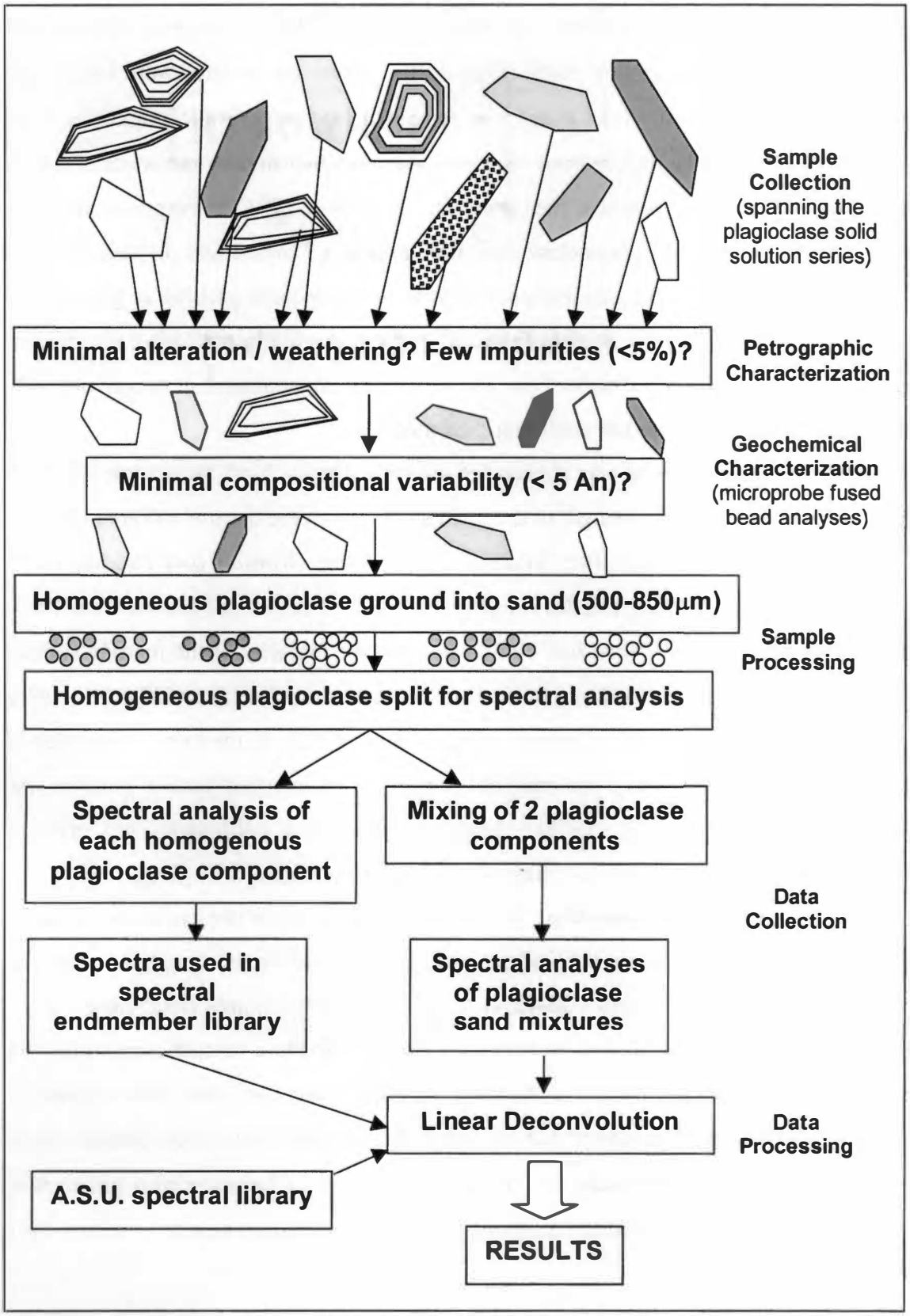

Figure 7. Flow chart showing procedures for Part II.

3.2.3. Sample Preparation. Selected plagioclases were individually ground into finer particles using mortar and pestle (Figure 7). These particulates were sieved and the coarse sand portion (500-850 μm) was separated for use. Visible impurities were extracted from each plagioclase sand. Samples were washed first by tap water and then de-ionized water. Each sand was then dried for 72 hours at 77^0 C to evaporate adhering water. Each homogenous plagioclase sand was thoroughly mixed and divided into two portions. Sand was mixed again and poured (with no subsequent packing of grains) into 3 cm diameter sample cups. Spectra from this portion were collected (using the spectral analysis technique described above) for use as spectral endmembers in deconvolutions. The second portion was used in preparing sand mixtures.

The coarse sand size was chosen for several reasons. First, particulate diameter must be kept above the wavelength of the incident energy in the thermal infrared to avoid particle size effects [*Lyon*, 1965; *Aronson et al.*, 1969, *Aronson and Emslie*, 1973; *Salisbury and Eastes*, 1985; *Salisbury and Wald*, 1992; *Moersch and Christensen*, 1995; *Mustard and Hays*, 1997; *Hamilton*, 1999]. Second, the majority of the martian surface has been shown to be covered by boulder to clay-sized particles [*Shorthill et al.*, 1976; *Dollfus and Deschamps*, 1986; *Christensen and Moore*, 1992], so the sample size used in this study is representative of the analyzed portion of the martian surface particle size distribution [*Shorthill et al.*, 1976]. Finally, coarse sand particulates are oriented randomly during spectral analyses, eliminating grain orientation effects [*Ruff*, 1998].

3.2.4. Mixture Preparation. In order to simulate coarse two-component zoning in plagioclase, homogeneous plagioclase sand components were mixed in measured proportions (75-25% / 50-50% / 25-75%) to produce sand mixtures (total mass ~3 g). Mixing of homogeneous plagioclase sands of distinct individual compositions produced compositional variances that are a function of plagioclase used and their respective volumes. A total of 21 mixtures that ranged in An variance (ΔAn) between the sands from ΔAn_{71} to ΔAn_9 were produced (Figure 8). Mixing of homogeneous plagioclase different sand mixtures produced a range of average plagioclase compositions from An_{14} to An_{71}.

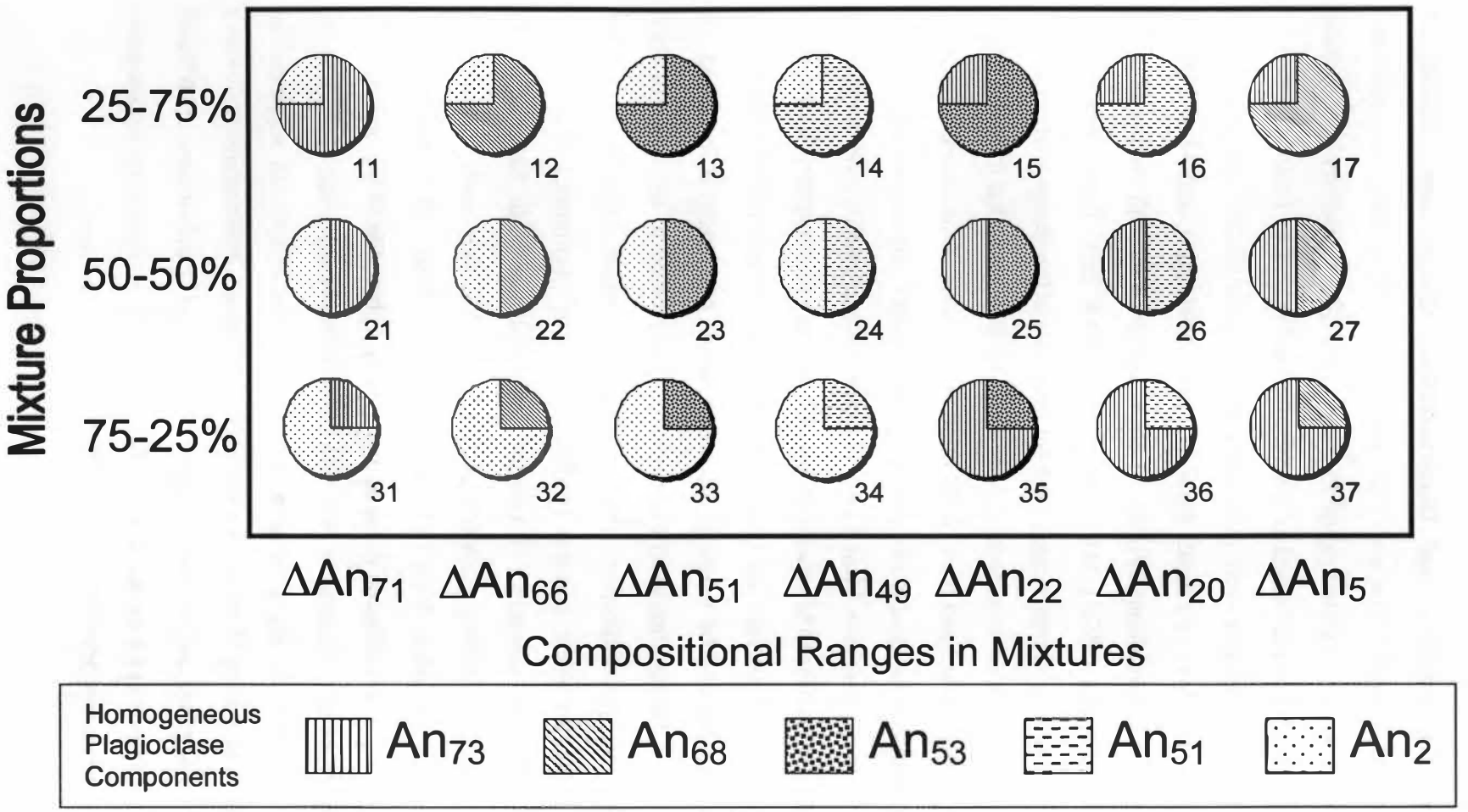

Figure 8. Matrix of two-component sand mixtures. Legend shows compositions of homogeneous plagioclase used in mixtures. Double digit #'s next to each pie chart refer to the mixture #'s.

3.2.5. Spectral Analyses and Deconvolutions. Spectra were collected as previously described, but with 270 scans of the spectrometer. They were then converted to emissivity according to the technique of *Ruff et al.* [1997]. Emissivity spectra were collected and deconvolutions performed as described in Section 3.1.4. Deconvolutions of plagioclase sand mixture spectra were performed at laboratory (2 cm^{-1} sampling), TES (10 cm^{-1} sampling), THEMIS (10 bands from 6-15μm wavelength), and Mini-TES (10 cm^{-1} sampling) spectral resolutions (Figure 9) allow comparison with results obtained from Mars Global Surveyor (MGS), Mars Odyssey, and MER data. For deconvolutions at THEMIS resolution, wavenumber ranges are not specified in the deconvolution as only 10 irregularly-spaced bands are available. Bands 9 and 10 were excluded from use due to effects of the CO_2 absorption band from the Martian atmosphere. With essentially only 8 THEMIS bands available for deconvolutions, only endmember sets containing 8 or less endmembers were used. Because Mini-TES will conduct observations over a variety of pathlengths, from centimeters to kilometers away, the effects of atmospheric components are less understood. At close viewing distances, bands around the 15μm CO_2 absorption feature to be excluded would be minimal. However, when pathlength is increased, the bands to be excluded during atmospheric correction are increased to the range of those excluded (825-507 cm^{-1}) in atmospherically corrected TES spectra. Thus, because Mini-TES and TES have the same spectral resolution (10 cm^{-1} sampling), TES spectra represent the "worst-case scenario" of viewing long distances with Mini-TES. To simulate some potential viewing pathlengths for Mini-TES, this study deconvolves mixture spectra over two other Mini-TES spectral ranges. First, 14 of the 30 bands between 825-507 cm^{-1} were excluded in equal amounts on either side of the 667 cm^{-1} (15 μm) CO_2 absorption band to simulate a 50% reduction in bandwidth, thus increasing the amount of bands available for deconvolution. It is assumed that this would represent the number of bands to be removed when viewing at some distance intermediate with views through the full atmosphere and at closest ranges. Secondly, all bands except at 667 cm^{-1} (15μm) CO_2 absorption band were included. This calibration is thought to represent the closest viewing distances of Mini-TES and thus the "best case scenario".

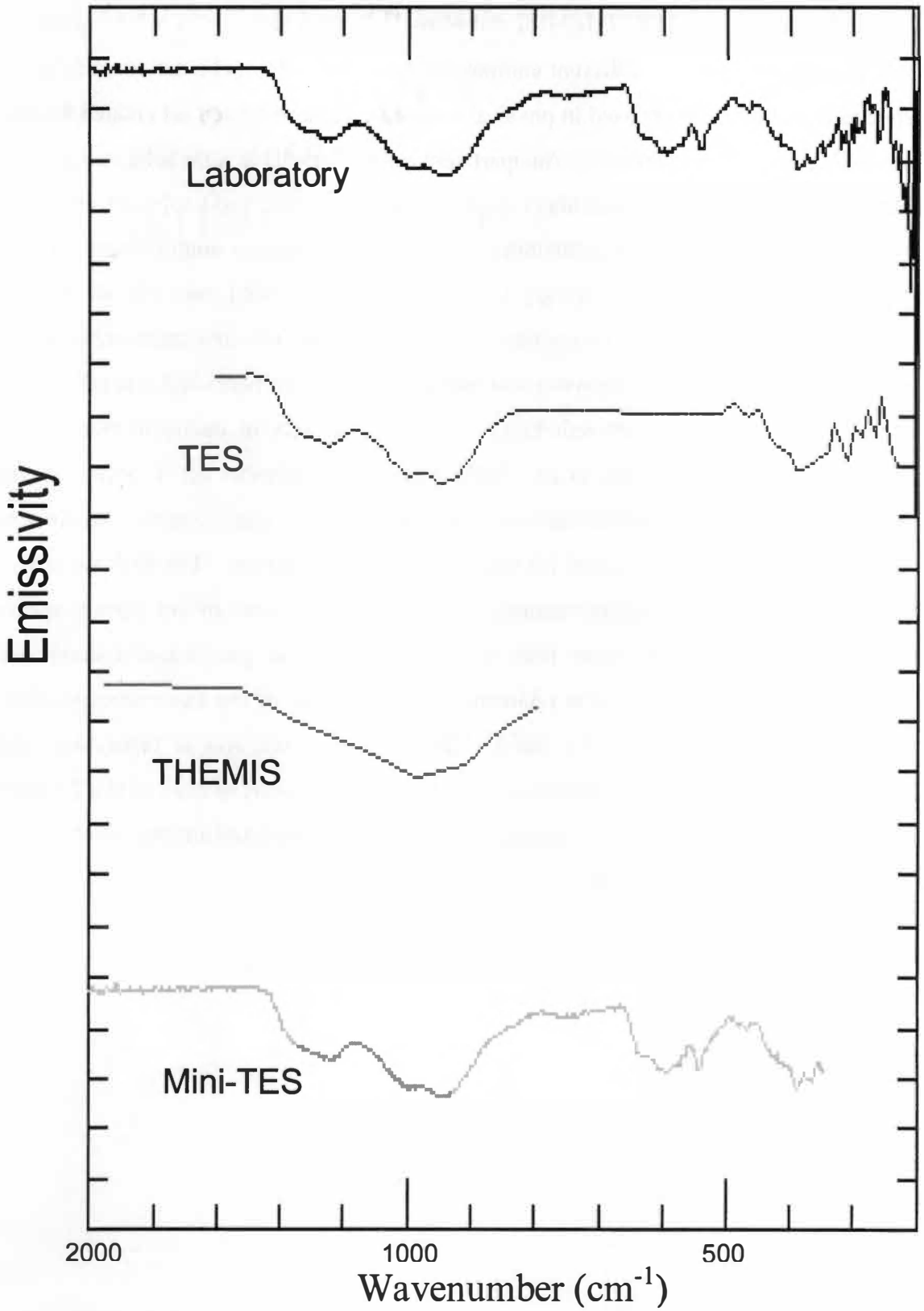

Figure 9. Example showing sand mixture 11 spectra at laboratory, TES, THEMIS, and Mini-TES (-CO_2 band). Spectra are offset 0.3 for clarity.

At laboratory, TES, THEMIS, and Mini-TES resolutions, each mixture spectrum was deconvolved using 5 different endmember sets (Table 5): (1) a set containing only spectra from endmembers used in physical mixtures, (2) a restricted set created by using spectral endmembers spaced ~15 An apart across the plagioclase solid solution series, (3) another restricted set of endmembers spanning the plagioclase solid-solution series from *Wyatt et al.* [2001], (4) a set containing all available plagioclase endmembers from this study and the ASU spectral library [*Christensen et al.*, 2000], and (5) all available plagioclase endmembers excluding those used in mixtures. The first endmember set was used as a "check" on the deconvolution technique. The two restricted sets (#2 and #3) were used to determine the suitability of using such sets in deconvolutions and to evaluate the use of the *Wyatt et al.* [2001] preferred endmember set in deconvolutions from Part I. The fourth endmember set represents the "best case" scenario, where some endmembers are an exact match for those present in the sample. The fifth set is more reflective of a realistic remote sensing scenario. The likelihood of our current spectral library containing endmembers that are exact matches of plagioclase compositions present at the martian surface is relatively low. This part of the experiment yielded a total of 483 deconvolutions for the 5 different endmember sets at laboratory, TES, THEMIS, and Mini-TES resolutions (Appendix G). The results of each of the 23 sets of deconvolutions were used to model average anorthite content (An) and modal abundance for each mixture (Appendix H).

Table 5. Plagioclase endmember sets used in deconvolutions from Part II. Samples labeled WAR are from Ward's Scientific, samples labeled BUR are from Burnham Scientific. Those without either designation are from this study.

Pure endmember sets*	15 An# spacing	[*Wyatt et al.*, 2001]	All plagioclase and Plagioclase-minus (**)	
A. 5851	WAR-0235	WAR-5851	WAR-0235**	1382a
1382	BUR-060D	WAR-5804	WAR-0244**	WAR-5759**
	WAR-0234	BUR-240	WAR-0612**	BUR-340**
B. 5851	WAR-1384	WAR-4524	5851	
SS	BUR-240	WAR-RGAND01	WAR-5851**	
	1382	WAR-5859	BUR-060D**	
C. 5851	BUR-340	BUR-340	BUR-060**	
4512		WAR-5759	WAR-5804**	
			WAR-3680**	
D. 5851			WAR-0234**	
0022			BUR-240**	
			WAR-3080A**	
E. 1382			WAR-0024**	
0022			4512A-L	
			0022b	
F. 1382			WAR-4524**	
4512			WAR-1384**	
			WAR-RGAND01**	
G. 1382			SS	
SS			WAR-5859**	
			1382a	
			WAR-5759**	

* = Endmember sets here are used for each column of the matrix in Figure 8. Example: endmember set A is used to deconvolve mixtures 11, 21, and 31

4. Results

4.1. Part I. Rocks: Phenocrysts vs. Groundmass

Microprobe analyses of rock samples (Appendix C) confirm that plagioclase phenocrysts are generally more calcic than groundmass plagioclase (Figure 10). Typically, measured plagioclase compositional ranges become more Na-rich (lower An) and compositionally variable with increasing bulk-rock wt% SiO_2. Compositional overlap among the grain types occurs as expected during fractional crystallization. Phenocrysts show a variety of zoning patterns (normal, reverse, oscillatory) that vary among and within rock samples. Normal zoning is present (calcic core to sodic rim material) but is not necessarily the dominant zoning pattern in most phenocrysts.

Microprobe analyses of the most anomalous rocks (HK-1, HK-3, HK-5), i.e., those whose modeled plagioclase compositions fell outside measured compositional ranges in the *Wyatt et al.,* [2001] study, reveal that all modeled values actually lie within the newly measured compositional ranges (Figure 10). In the previous study [*Wyatt et al.*, 2001], the tendency to analyze larger grains led to more restricted plagioclase compositional ranges than are actually present. With larger grains typically being more Ca-rich, these analyses excluded more of the Na-rich plagioclase. Spectrally modeled values correlate well with the compositional range of the dominant grain type in each sample (Figure 10). In other words, in most samples the mesostasis plagioclase has the highest areal (volume) percentage and so most modeled values are found to coincide with reported plagioclase mesostasis compositional ranges. In the few cases where plagioclase phenocrysts dominate, modeled values fall within measured plagioclase phenocryst compositional ranges. Sample 79-3b contains sodic groundmass plagioclase and a separate, non-overlapping assemblage of plagioclase phenocrysts (possibly xenocrysts), as illustrated in Figure 10. Although the modeled value for this sample falls within the measured compositional range for the dominant grain type (mesostasis in this case), this introduces the possibility of average compositions lying outside measured compositional ranges. Thus, modeled values may represent an average plagioclase composition for a sample, but could potentially represent a composition not actually present in the rock.

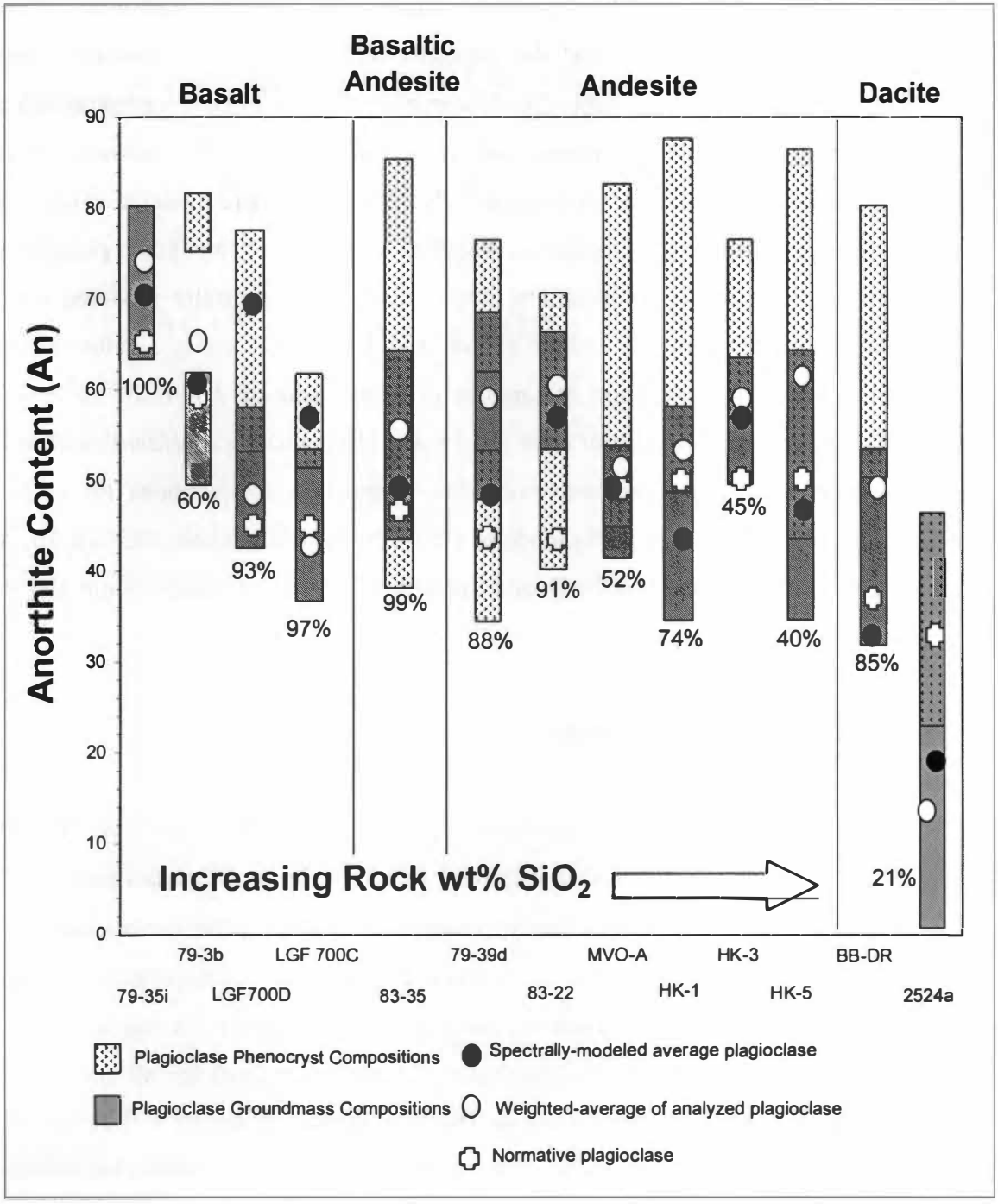

Figure 10. Part I: Modeled plagioclase compositions plotted against weighted average and CIPW NORM-calculated average plagioclase compositions for each rock sample. The x-axis shows increasing rock wt% SiO_2, while the y-axis indicates anorthite content (An). Percentages indicate the total plagioclase that is groundmass. Sample numbers are also shown along the x-axis. Rock wt% SiO_2 are relative.

Although spectrally modeled values lie within measured plagioclase compositional ranges, modeled An generally remains lower than median plagioclase compositions (Figure 10; Table 2). Because median plagioclase compositions are not representative of average plagioclase compositions for rocks, average plagioclase compositions for each rock were needed. In order to compare modeled values with true average plagioclase compositions, weighted averages of analyzed plagioclase and normative plagioclase compositions were calculated. Spectrally modeled plagioclase compositions are typically within +10/-6 An of weighted average values (Figure 10; Table 2), with the exception of samples LGF700D and BB-DR (+20/-16 An), mostly within the reported margins of error (10-15 An) of the technique [*Hamilton et al.*, 2001]. However, when compared with normative plagioclase compositions for each sample (Figure 10; Table 2), spectrally modeled values are typically within +13/-14 An, with the exception of samples LGF700D and BB-DR (+25/-14 An), also within the reported margins of error (10-15 An).

4.2. Part II: Plagioclase zoning

Analyses of the two-component sand mixtures at laboratory, TES, THEMIS, and Mini-TES resolutions show that measured vs. spectrally modeled compositions display linear trends (Figures 11-12). Anorthite variances (ΔAn) for the various deconvolutions are shown in Appendix H. Deconvolved plagioclase compositions at laboratory resolution (2 cm^{-1} sampling) can be modeled to within +9/-11 An and to within +9/-12 An of measured values at TES resolution (10 cm^{-1} sampling) for all endmember sets. Modeled plagioclase compositions at THEMIS resolution are to within +17/-9 An of measured values. When deconvolutions of physical mixtures involving albite, whose structural disorder (low vs. high order albite) leads to problems during linear deconvolutions [*Ruff*, 1998], are excluded, modeled compositions lie within +6/-8 An, +3/-8 An, and +11/-6 An of measured values for laboratory, TES, and THEMIS resolutions respectively (Figures 13-14) for all endmember sets. Deconvolutions using

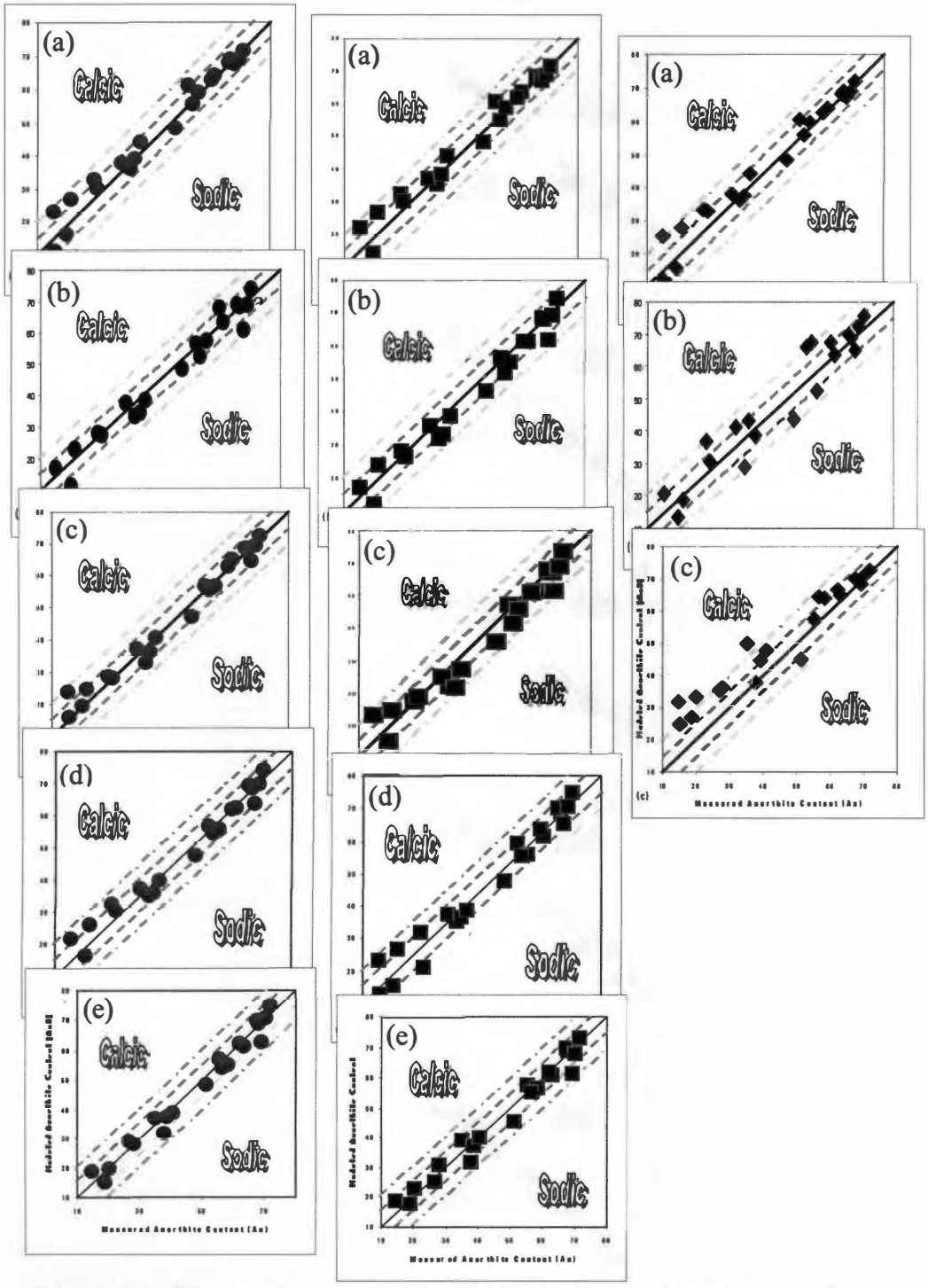

Figure 11. Measured vs. modeled plagioclase compositions deconvolved at laboratory (column 1), TES (column 2), and THEMIS (column 3) resolution using: (a) only plagioclase used in mixtures, (b) plagioclase endmembers spaced 15 An apart, (c) [*Wyatt et al.*, 2001] endmember set, (d) all available plagioclase*, and (e) all available plagioclase except those used in mixtures*. * = not used in THEMIS deconvolutions

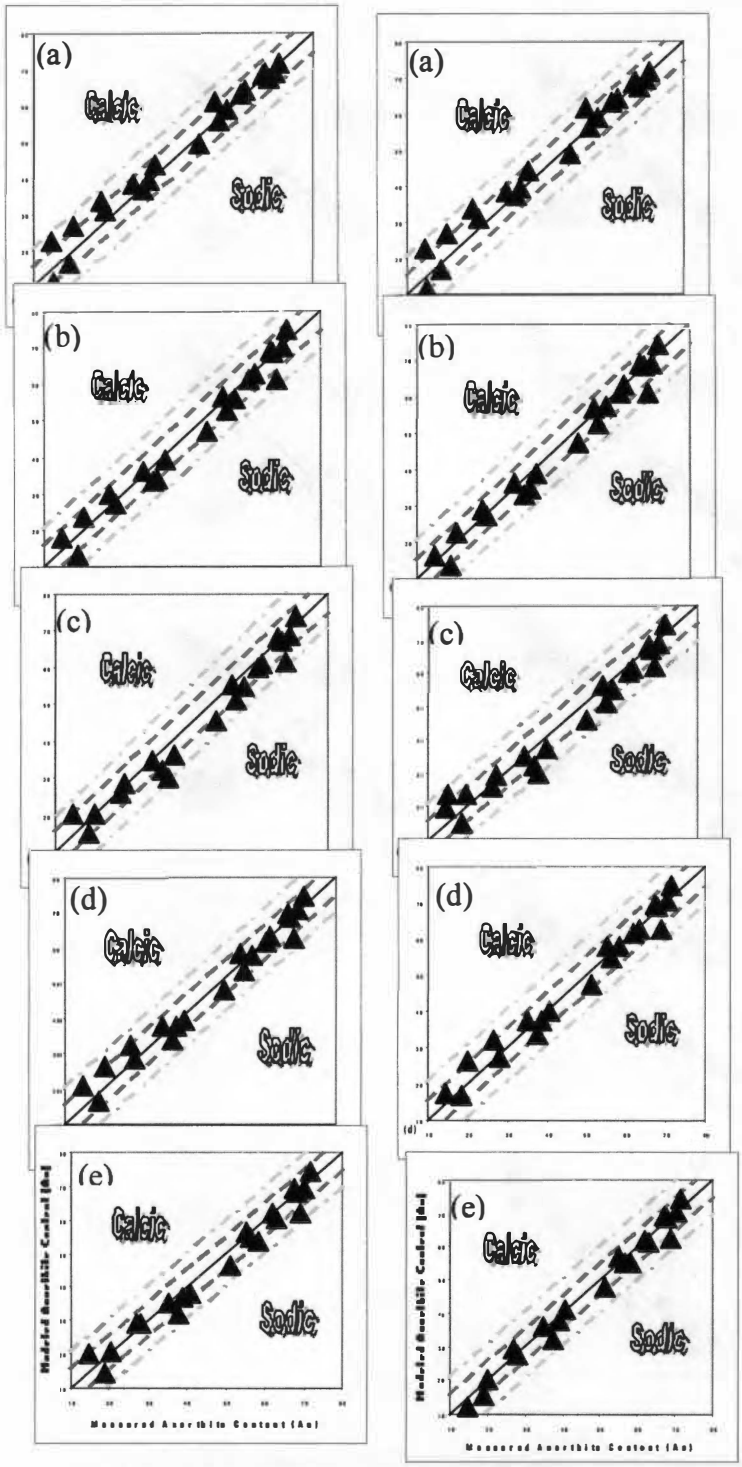

Figure 12. Measured vs. modeled plagioclase compositions deconvolved at Mini-TES resolution (with 50% of TES CO_2 bands removed – column 1 and only 15μm CO_2 band removed – column 2) using: (a) only plagioclase used in mixtures, (b) plagioclase spaced 15 An apart, (c) [*Wyatt et al.*, 2001] endmember set (d) all available plagioclase, and (e) all available plagioclase except those used in mixtures.

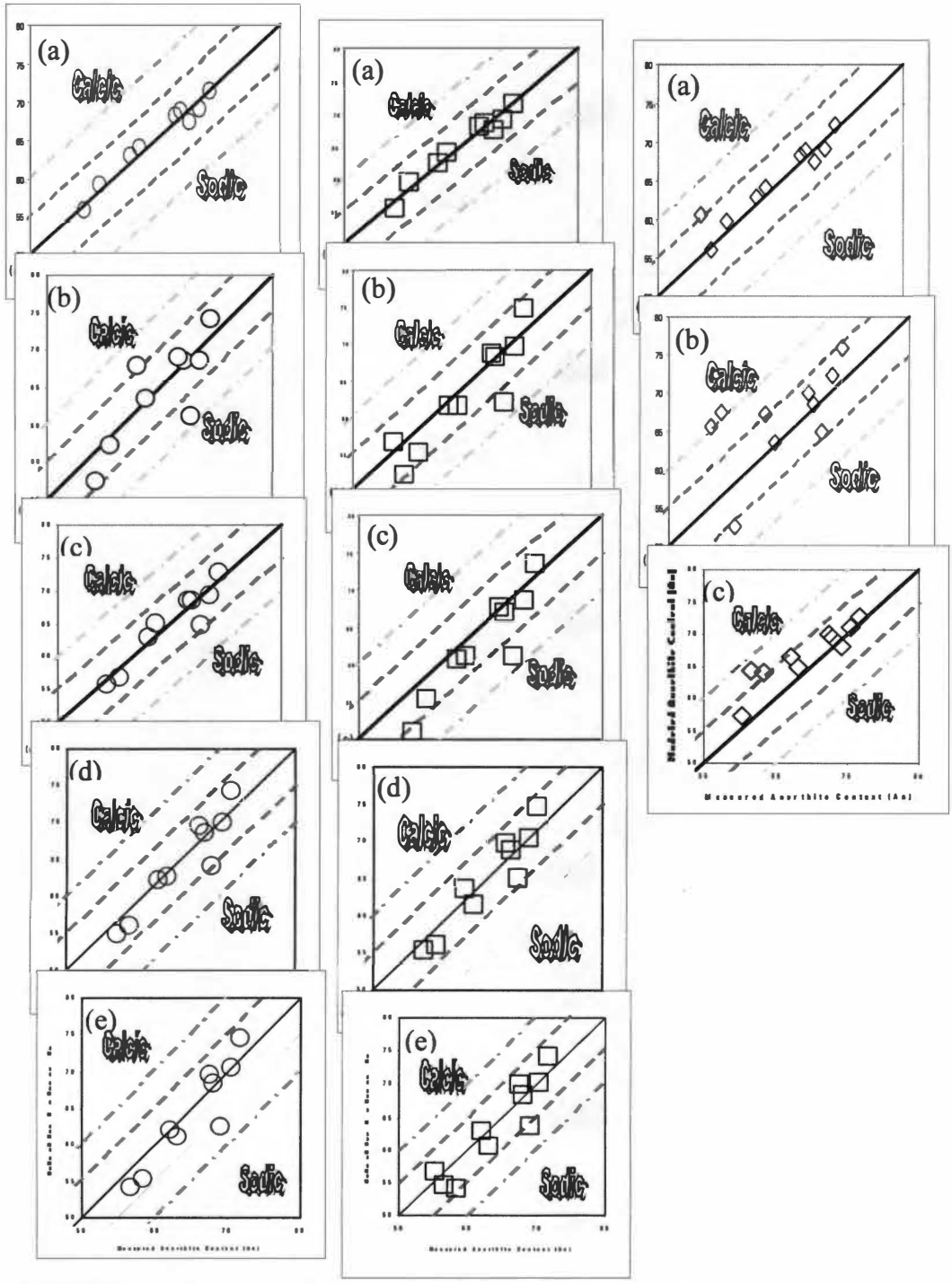

Figure 13. Measured vs. modeled plagioclase compositions deconvolved at laboratory (column 1), TES (column 2), and THEMIS (column 3) resolution (without mixtures involving albite) using: (a) only plagioclase used in mixtures, (b) plagioclase endmembers spaced 15 An apart, (c) [*Wyatt et al.*, 2001] endmember set, (d) all available plagioclase*, and (e) all available plagioclase except those used in mixtures*. * = not used in THEMIS deconvolutions

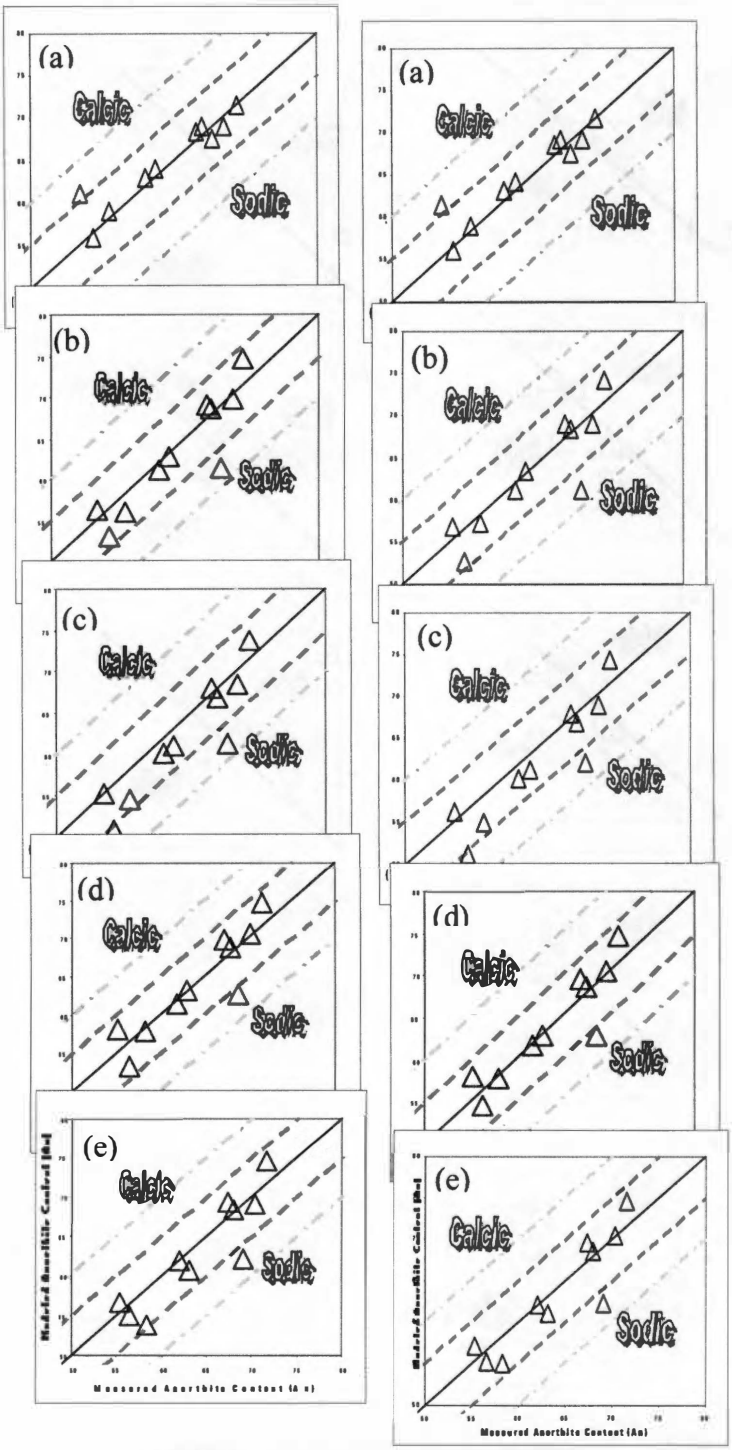

Figure 14. Measured vs. modeled plagioclase compositions deconvolved at Mini-TES resolution (without mixtures involving albite and with 50% of TES CO_2 bands removed – column 1 and only 15μm CO_2 band removed – column 2) using: (a) only plagioclase used in mixtures, (b) plagioclase spaced 15 An apart, (c) [*Wyatt et al.*, 2001] endmember set (d) all available plagioclase, and (e) all available plagioclase except those used in mixtures.

the various endmember sets also model both calcic and sodic plagioclase in sub-equal amounts. For the two sets of deconvolutions at Mini-TES resolution, modeled anorthite are within +8/-12 An (50% of bands removed) and +8/-11 An (all but 15 μm CO_2 band present) of measured average plagioclase compositions (Figure 12). When mixtures involving albite are excluded (Figure 14), precision improves to within +3/-8 An for both sets of deconvolutions including all endmembers.

5. Discussion

Plagioclase phenocrysts and groundmass in terrestrial volcanic rocks in this study display a variety of zoning patterns (normal, oscillatory, reverse) and normal zoning cannot be assumed as typical. Thus, assuming that more sodic-modeled plagioclase compositions are the result of the volumetric dominance of increasingly more sodic rims in plagioclase dominated by normal zoning [*Wyatt et al.*, 2001] is incorrect. Microprobe measurements also extend the plagioclase compositional ranges for the most anomalous samples from the *Wyatt et al.* [2001] study. By not sampling the full range of plagioclase grain types, from phenocrysts to the smallest of groundmass, not all modeled values in the *Wyatt et al.* [2001] study corresponded to measured compositional ranges. This gave the appearance that the linear deconvolution technique was not accurately modeling plagioclase compositions.

Part I results suggest that the sodic trend (as compared to median plagioclase compositions) in spectrally modeled plagioclase compositions arises from the contribution of the areally (volumetrically) more abundant grain type in each sample. In most cases, a more sodic plagioclase groundmass dominates, shifting the modeled An to more sodic ends of the compositional range. In all cases modeled plagioclase compositions correspond to the dominant grain type, reaffirming that linear mixing of the spectra of plagioclase phenocrysts and groundmass occurs. Thus, samples with plagioclase dominated by a mesostasis will have more sodic modeled average plagioclase compositions. Although the opposite is true in specimens dominated by plagioclase phenocrysts, most samples from this study (and probably most volcanic rocks) are dominated by groundmass plagioclase, producing spectrally modeled plagioclase compositions that are more sodic than median compositions.

When spectrally modeled average plagioclase compositions are related to standards of comparison (weighted averages and normative plagioclase), most results are consistent with previous studies [*Hamilton et al.*, 2001]. Modeled plagioclase compositions are to within +10/-6 An of weighted average plagioclase and +13/-14 An of normative plagioclase compositions. One of the samples that is an exception to this is LGF700D, which appears to have experienced a higher degree of weathering, as

compared to other rocks used in this study. Because of this, the *Wyatt et al.* [2001] endmember set may not be as suitable for modeling weathered volcanic rocks. Related to this, *Wyatt et al.* [2002] developed a new endmember set used to model TES spectra from weathered rocks Mars. As shown earlier, the comparison of modeled plagioclase compositions to normative plagioclase is less precise than comparison to weighted average compositions. This is likely due to the assumption used in CIPW-NORM calculations of plagioclase in equilibrium with the remaining melt during fractional crystallization. Plagioclase zoning results from non-equilibrium conditions during crystallization, making this assumption problematic. Thus, use of normative plagioclase as a standard of comparison may be invalid. Plagioclase compositions can be modeled to higher precision as compared weighted average plagioclase compositions as a standard of comparison. Errors of +10/-6 An are comparable to modeled plagioclase compositions from sand spectra, including mixtures involving albite. No matter which standard modeled compositions are compared to, it is uncertain which standard is truly more representative of average plagioclase compositions in a rock.

Weighted compositions were calculated form microprobe analyses in which core to rim transects (in subequal intervals) were made across representative plagioclase phenocryst and groundmass grains. The number of analyses ranged from 8-15 (phenocrysts) and 2-5 (groundmass grains). Plagioclase zoning patterns within single samples include normal, reverse, oscillatory, and combinations of these. Weighted average compositions were calculated by separately averaging microprobe analyses from plagioclase phenocrysts and groundmass grains. Calculations assumed that traverse analyses were representative of areal exposures of zones in plagioclase. This assumption presents some level of uncertainty to weighted average compositions, however. This is demonstrated by considering a hypothetically zoned circular plagioclase grain (100μm diameter) having 10 zones, each 10 μm in width, with normal zoning. Zones range from An_{75}-An_{54} in composition (typical range for terrestrial plagioclase). For this example, it is assumed that 10 microprobe analyses were made in a core to rim transect, with each analysis corresponding to an individual zone. The weighted average plagioclase composition (An_{63}) was calculated for this grain using the previously described method.

Taking into account the actual areal exposure (area of a circle) for each zone, a 'new' weighted average composition of An_{59} was determined. Examining the same grain, but reversely zoned, reveals a plagioclase composition of An_{67}. Similar calculations with other normal and reversely zoned (zones of variable thickness) hypothetical plagioclase grains yield similar results. This suggests that for a single grain, weighted average compositions from the original method can be predicted to within $\pm$ 4 An. It these examples, it is assumed that actual areal exposures dominate over volume considerations. This reasoning relates to the electron microprobe and spectrometer primarily measuring energy from the surface of each sample. Penetration depths for the electron microprobe are typically <10μm and <30μm for the spectrometer, with the majority of the spectra coming from the topmost layers of the sample.

While both of these examples demonstrate the approximate level of uncertainty involved in calculating weighted average compositions, the margin of error is relatively low ($\pm$4 An). With such variability in zoning patterns within a given sample, it is assumed that the variability serves to 'even out' the margins of error of calculations used in this study. Despite such variability, many whole rocks show normal zoning trends overall. Such being the case, weighted average compositions as calculated in this study could be overestimated as being more calcic than those calculated taking into consideration areal exposures. Based on the previous hypothetical example, this overestimation could be as much as +4 An. If this is true, then plagioclase compositions can be modeled to within +6/-2 An of weighted average plagioclase, suggesting even better precision than the previously reported margin of error (+10/-6 An) for most samples and comparable to modeling precision in 'simulated zoned' zoned samples from Part II.

Results from Part II indicate that physical mixtures of homogenous plagioclase components produce a composite spectrum that is representative of the average plagioclase composition for that given sample. Deconvolutions of sand mixtures at laboratory, TES, THEMIS, and Mini-TES resolutions confirm this. In other words, the volumetric domination of more sodic zones in a normally-zoned plagioclase will yield a spectrum that is representative of a more sodic average plagioclase composition. A

reversely-zoned plagioclase with volumetrically dominant calcic zones will yield a spectrum that is representative of a more calcic average plagioclase composition. In addition, linear deconvolutions of spectra from such mixtures produce modeled compositions that approximate average plagioclase compositions better than previously reported [*Hamilton et al.*, 2001]. While reported margins of error for all mixtures using all endmember sets at laboratory, TES, THEMIS, and Mini-TES resolutions were modest, precision can be improved further by choice of endmember set input into the deconvolution algorithm. Endmember sets were evaluated for their overall ability to determine average plagioclase compositions at all resolutions by comparison of ΔAn (anorthite content variance) among different endmember sets and also by similar comparison of standard deviations from deconvolutions (Table 6). Excluding the pure endmember sets that serve as a "check" to deconvolutions, the evaluation reveals that better results are achieved by use of endmember sets with a higher number of spectral endmembers (i.e. all available plagioclase or all available plagioclase minus those used in the mixtures). More restricted endmember sets (sets #2 and 3) produce higher ΔAn values and standard deviations.

Better precision is also reached when considering plagioclase mixtures not involving albite. The structural disorder between low and high-order albites and the presence of a significant K component in albite poses problems for linear deconvolutions as outlined in *Ruff* [1998]. At laboratory, TES, THEMIS, and Mini-TES resolutions, average plagioclase compositions in albite-free mixtures can be modeled to within +6/-8 An, +3/-8 An, +11/-6 An, and +3/-8 An respectively. Again, results can also be improved depending upon which endmember set is used in the linear deconvolution algorithm. By careful selection of endmember sets (excluding set #1), results of +2/-5 An, +3/-4 An, +8/-1 An, and +3/-6 An can be achieved for laboratory, TES, THEMIS, and Mini-TES resolutions. Endmember sets used in deconvolving mixtures not involving albite were evaluated by the method previously described. Results again indicate that endmember sets involving more plagioclase spectral endmembers lead to better precision in determining average plagioclase compositions.

Table 6. Plagioclase compositional variations for deconvolutions at laboratory, TES, THEMIS, and Mini-TES resolutions.

Resolution	Embr	(+An)	(-An)	IΔAnI	St Dev	Resolution	Embr	(+An)	(-An)	IΔAnI	St Dev
LAB	Pure	8	-4	12	1.87	*LAB*	Pure	1	-2	3	0.67
	15 An sp.	6	-11	17	2.32	*(-albite)*	15 An sp.	6	-8	14	2.01
	Wyatt	9	-5	14	1.56		*Wyatt*	2	-5	7	1.04
	AllPLAG	7	-5	12	1.91		AllPLAG	3	-5	8	1.21
	AllMinus	4	-9	13	1.84		AllMinus	3	-6	9	1.57
TES	Pure	8	-6	14	1.94	*TES*	Pure	1	-2	3	0.61
	15 An sp.	4	-12	16	2.34	*(-albite)*	15 An sp.	3	-7	10	1.71
	Wyatt	8	-8	16	2.45		*Wyatt*	2	-8	10	1.92
	AllPLAG	9	-7	16	2.20		AllPLAG	3	-4	7	1.35
	AllMinus	6	-8	14	2.11		AllMinus	3	-5	8	1.64
THEMIS	Pure	11	-3	14	2.11	*THEMIS*	Pure	1	-1	2	0.71
	KM-sub	11	-9	20	3.68	*(-albite)*	KM-sub	11	-6	17	2.81
	MV	17	-6	23	4.30		MV	8	-1	9	2.12
MINI-TES	Pure	8	-4	12	1.87	*MINI-TES*	Pure	1	-2	3	0.64
(50% Rem.)	15 An sp.	4	-12	16	2.19	*(50% Rem.)*	15 An sp.	3	-8	11	1.61
	Wyatt	5	-9	14	2.34	*(-albite)*	*Wyatt*	2	-8	10	2.11
	AllPLAG	6	-7	13	2.04		AllPLAG	3	-6	9	1.35
	AllMinus	6	-9	15	2.04		AllMinus	3	-7	10	1.72
MINI-TES	Pure	8	-4	12	1.85	*MINI-TES*	Pure	1	-2	3	0.64
(ALL-CO_2)	15 An sp.	3	-11	14	2.01	*(ALL-CO_2)*	15 An sp.	3	-8	11	1.58
	Wyatt	8	-9	17	2.44	*(-albite)*	*Wyatt*	3	-7	10	1.96
	AllPLAG	6	-6	12	1.80		AllPLAG	3	-6	9	1.23
	AllMinus	3	-9	12	1.67		AllMinus	3	-7	10	1.52

Embr. Set	Pure	15An#	Wyatt	ALL	AM	Embr. Set	Pure	15An#	Wyatt	ALL	AM
Avg IΔAnI	12.5	15.8	15.25	13.25	13.5	Avg IΔAnI	3	11.5	9.25	8.25	9.25
Ranking	1	5	4	2	3	Ranking	1	4	3	2	3
	Pure	15An#	Wyatt	ALL	AM		Pure	15An#	Wyatt	ALL	AM
Avg St Dev	1.88	2.21	2.20	1.99	1.91	Avg St Dev	0.64	1.72	1.76	1.29	1.61
Ranking	1	5	4	3	2	Ranking	1	4	5	2	3

Rankings: 1=best 5==worst

Resolution	LAB	TES	THEMIS	Mini-TES	Mini-TES	Resolution	LAB	TES	THEMIS	Mini-TES	Mini-TES
Avg IΔAnI	14	15.50	21.5	14.5	13.75	Avg IΔAnI	9.5	8.75	13	10	10
Ranking	2	4	5	3	1	Ranking	1	3	4	2	2
	LAB	TES	THEMIS	Mini-TES	Mini-TES		LAB	TES	THEMIS	Mini-TES	Mini-TES
Avg St Dev	1.91	2.28	3.99	2.15	1.98	Avg St Dev	1.46	1.66	2.47	1.70	1.57
Ranking	1	4	5	3	2	Ranking	1	3	5	4	2

While errors in the deconvolution are reported as +/- An (Table 6), standard deviation is another means of measuring the degree of error involved. Errors reported as +/- An represent the maximum amount of error for either a single set of deconvolutions or for the entire set at a particular resolution (as shown above). This form of reporting includes the most poorly modeled values and may not represent the majority of modeled plagioclase compositions for deconvolutions involving a particular endmember set or at a given spectral resolution. Standard deviations are more representative of the majority of measured vs. modeled plagioclase compositions using a particular endmember set or at a particular spectral resolution. For example, although, in mixtures not involving albite, plagioclase compositions can be modeled to within +6/-8 An, +3/-8 An, +11/-6 An, and +3/-8 An of measured values at lab, TES, THEMIS, and Mini-TES resolutions respectively, the majority of modeled compositions were to within ± 2 An at lab, TES, and Mini-TES resolutions and to within ± 3 An at THEMIS resolution (Table 6).

Analysis of spectral endmembers used in deconvolutions of sand mixtures provides no definite characteristic features that indicate the true number and abundances of zones (2) present. Although many spectral endmembers selected by the deconvolution algorithm correspond closely to those present within each mixture, significant percentages of others do not. This would suggest the presence of more than two zones. Although precision in determining plagioclase compositional variability is slightly improved with the addition of more spectral endmembers (sets 4 and 5), significant proportions (>10%) of compositionally different endmembers are still chosen by the algorithm. Perhaps by the continued addition of spectral endmembers at every 1 An interval over the entire plagioclase solid solution series, future deconvolutions will allow the identification of distinct clusters of endmembers that correspond with compositions of the dominant plagioclase zones in a rock. However, with most volcanic rocks containing multiple plagioclase zones of a whole range of compositions, the identification of zones by identification of clusters of spectral endmembers may be difficult if not impossible.

This study involved use of albite as a component of sand mixtures to simulate a "worst case scenario" for rocks involving a strong albite component to plagioclase. In the case of Mars, the two most dominant derived surface types have been interpreted as

basalt and either andesite or weathered basalt. Based on known plagioclase compositions from terrestrial basalts and andesites, most plagioclase compositions are $>An_{30}$. Plagioclase (maskelynite) compositions in most martian meteorites [e.g. *McSween and Treiman*, 1998; *Zipfel et al.*, 1999; *Folcho & Franchi*, 2000; *Rubin et al.*, 2000; *Taylor et al.*, 2000; *Zipfel*, 2000; *Ikeda et al.*, 2002, *Imae et al.*, 2002; *Lin et al.*, 2002; *Mikouchi & Miyamoto*, 2002; *Yanai*, 2002;] show ranges comparable to terrestrial basalts. Based on martian meteorite compositions, it is assumed that most exposed rocks at the martian surface have plagioclase with compositions above An_{30}. Thus, sand mixtures not involving albite are more representative of most plagioclase exposed on the martian surface. This suggests that with careful selection of endmember sets, TES, THEMIS, and Mini-TES have the potential to model average plagioclase compositions to within +3/-4 An, +8/-1 An, and +3/-6 An.

The relative higher imprecision in determining average plagioclase compositions from rock samples vs. those determined from sand mixtures arises from uncertainty in knowing whether either weighted average or normative plagioclase represent the true average plagioclase composition for each sample. When compared to modeled plagioclase compositions, normative plagioclase is often more sodic and weighted average plagioclase compositions are often more calcic, suggesting that either standard may be biased from the actual average plagioclase in all samples. As mentioned earlier, CIPW-NORM calculations assume equilibrium between crystals and melt during crystallization. Zoned minerals, quite common in volcanic rocks, indicate non-equilibrium conditions. This suggests that normative calculations for volcanic rocks produce average plagioclase compositions in error. Weighted average plagioclase compositions were calculated assuming that core-to-rim transects across individual grains were representative of the areal percentage of zones exposed at the rock's surface and are likely to be more representative of true average plagioclase compositions. Thus, the relative lack of precision in rocks vs. sand may not be that pronounced.

6. Applications to Martian Remote Sensing

Results from this study demonstrate the confidence with which TES, THEMIS, and Mini-TES spectra can be deconvolved to derive plagioclase compositions. These results have various applications to petrogenetic, geospatial, morphological, and hydrological studies of Mars. The ability to detect variations in plagioclase compositions can be used to discriminate between different lava flows, identify source regions for landing site samples, compare global and regional martian plagioclase compositions to martian meteorites, and identify areas of subaqueous or hydrothermal alteration of basalts/andesites.

In terrestrial volcanic centers, magmatic compositions often vary with time, the degree of source region melting, fractional crystallization, assimilation, etc. Such evolution is expressed in the compositional variability of lava flows. Analysis of TES, THEMIS, and Mini-TES thermal emission spectra might be used to identify compositionally distinct flow/rock units on the martian surface by their plagioclase compositions. Using TES and Mini-TES data to determine anorthite contents and THEMIS data to produce detailed maps of such units may provide a means of tracking the evolution of martian magmas. Studies of lava flows with more variable average plagioclase compositions (more than 10-15 An) would be better suited for use because of precision errors in modeling rock compositions (shown in Part I: Results). Deconvolved plagioclase compositions can also be used to measure compositional variability of laterally extensive lava flows on Mars. Terrestrially, flow bulk compositions not only vary by eruptive episode, but by proximity to the eruptive center. Plagioclase compositions can also provide crystallization temperature information and have the potential for use as geobarometers [*Coskren & Blackburn*, 1972; *Nash*, 1973]. Such information have the potential to provide insight into emplacement processes and crystallization depths.

Another potential application also involves data sets from both orbiters (MGS & Odyssey) and landers (MER rovers). Mini-TES will presumably collect spectra from individual rocks that were derived from various geologic units. With Mini-TES's

potential to discriminate plagioclase compositions to within +3/-6 An (in rocks without albite), these data can be compared to plagioclase compositions detected at the landing site by TES and THEMIS from orbit. Thus, source beds for individual rocks observed at landing sites might be identified, allowing geologic interpretation of an area beyond the short traverses of the MER rovers.

Deconvolutions of Surface Type 1 and Surface Type 2 spectra from Mars also provide insight into variability of martian surface rocks (Table 7). Deconvolutions of spectra using endmember sets from *Wyatt et al.* [2001], *Wyatt & McSween* [2002], plagioclase spaced 15 An apart, and all available plagioclase from this study reveal varying plagioclase compositions among both surface types. Modeled plagioclase compositions for Surface Type 1 range from An_{66}-An_{42} and range from An_{60}-An_{34} for Surface Type 2. Derived compositions suggest that, when compared to terrestrial and lunar basalts (Figure 15), martian basalts (from Mars meteorite and deconvolved compositions) are relatively depleted in Ca and enriched in volatiles (Na and K). This is consistent with studies by *Wanke and Dreibus* [1988] and *Papike* [1998] showing enrichments in Na and K. This suggests that: martian magmas are distinct from lunar and terrestrial basaltic magmas, martian magmas are much more evolved, and/or that Martian meteorites and spectrally derived basalts have been extensively altered.

Igneous rocks comprise a majority of the Earth's surface area (subaerial and subaqueous) largely as basalts in the oceanic crust. The exposure of basalts to seawater results in aqueous alteration of tholeiitic basalts into spilites, whose plagioclase feldspar has been albitized and other minerals altered to produce a greenschist-like assemblage. Similar alteration occurs in hydrothermal systems and as a result of metasomatism. Albitization is thought to occur by these reactions:

$$2Na^+ + CaAl_2Si_2O_8 + 4SiO_2 \longrightarrow 2NaAlSi_3O_8 + Ca^{2+}$$

or

$$1.5CaAl_2Si_2O_8 + Na^+ + 2H^+ \longrightarrow NaAlSi_3O_8 + 1.5Ca^{2+} + Al_2O_3 + H_2O$$

[*Rosenbauer et al*, 1988]. Albitization is quite common in oceanic basalts [e.g. *Hardie*, 1983; *Alt & Emmerman*, 1985; *Stakes & Schiffman*, 1999] and hydrothermally-altered basalts near volcanic centers on continents [*Whyte*, 1966]. If martian igneous rocks have

Table 7. Deconvolved plagioclase compositions from Surface Type I and II spectra.

Endmember set	Surface Type 1	Surface Type II
All plagioclase	An_{42}	An_{34}
15 An spacing	An_{47}	An_{34}
[*Wyatt et al.*, 2001]	An_{61}	An_{59}
[*Wyatt et al.*, 2002]	An_{66}	An_{60}

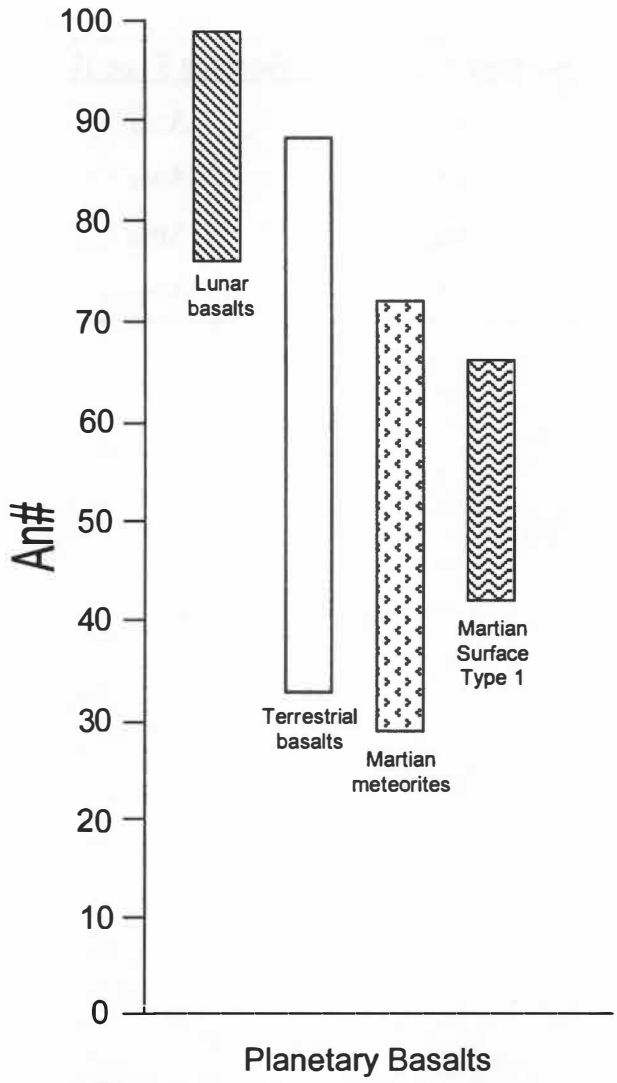

Figure 15. Plagioclase compositions for lunar, terrestrial, and martian basalts.

plagioclase typically > An_{30}, we can infer that more sodic plagioclase compositions ~<An_{20} have likely experienced some degree of alteration. Identification of albitized surfaces on Mars may indicate former sites of magmatic or hydrothermal fluids or the presence of marine environments.

7. Summary

Detailed geochemical and spectral analyses of plagioclase-rich rocks and plagioclase sand mixtures have provided new insight into martian remote sensing capabilities and the potential for further investigations. Results from this study have revealed that:

- Zoning patterns in volcanic rocks are highly variable and thus, do not exert an overriding influence on modeled average plagioclase compositions;
- Measured plagioclase compositional ranges from the *Wyatt et al.* [2001] study did not represent the complete plagioclase compositional range present within rock samples;
- Sodic groundmass plagioclase is the dominant grain type in most terrestrial volcanic rocks and thus has a greater influence on thermal emission spectra that are used to model average plagioclase compositions;
- Spectrally-modeled plagioclase compositions are primarily within +10/-6 and +13/-14 An of weighted average and normative plagioclase compositions respectively;
- Plagioclase "zones" from sand mixtures add together linearly to produce composite spectra representative of average plagioclase compositions for each mixture;
- Deconvolutions of sand mixtures suggest that laboratory TES, THEMIS, and Mini-TES instruments can predict modeled plagioclase compositions to within +6/-8 An, +3/-8 An, +11/-6 An, and +3/-8 An of measured values.

Spectra from complex mixtures of plagioclase, involving either/both groundmass and phenocryst plagioclase or zones within plagioclase grains, linearly mix to produce a rock/mineral spectrum that reflects the average plagioclase composition. So in rocks and sand mixtures involving complex mixtures of grains of variable compositions/abundances

and grains with variable intergranular zoning patterns, average plagioclase compositions can be accurately derived. With such results, this study provides an increased level of confidence in discerning martian plagioclase compositions and provides scientists with a new evaluative tool for examining a variety of martian geologic processes.

LIST OF REFERENCES

Alt, J. C. and r. Emmermann, Geochemistry of hydrothermally altered basalts: Deep Sea Drilling Project Hole 504B, Leg 83, *Initial Reports of the Deep Sea Drilling Project, 83,* 249-262, 1985.

Aronson, J. R., L. H. Bellotti, and R. K. McConnell, Jr. Radiative transfer in minerals at temperatures up to 1723 degrees K, *Eos, 50*, 315, 1969.

Aronson, J. R. and Emslie, A. G., The prospects for mineral analysis by remote infrared spectroscopy, *The Moon, 5*, 3-15, 1972.

Bandfield, J. L., V. E. Hamilton, and P. R. Christensen, A global view of Martian surface compositions from MGS-TES, *Science, 287*, 1626-1630, 2000a.

Bandfield, J. L., M. D. Smith, and P. R. Christensen, spectral dataset factor analysis and end-member recovery: Application to analysis of Martian atmospheric particulates, *J. Geophys. Res., 105*, 9573-9587, 2000b.

Bibring, J. P., M. Combes, Y. Langevin, A. Soufflot, C. Cara, P. Drossart, Th. Encrenaz, S. Erard, O. Forni, B. Gondet, L. Ksanfomality, E. Lellouch, Ph. Masson, V. Moroz, F. Rocard, J. Rosenqvist, and C. Sotin, Results from the ISM experiment, *Nature, 341*, 591-593, 1989.

Bibring, J. P., S. Erard, B. Gondet, Y. Langevin, A. Soufflot, M. Combes, C. Cara, P. Drossart, T. Encrenaz, E. Lellouch, J. Rosenqvist, V. I. Moroz, A. V. Dyachkov, A. V. Gryogoriev, N. G. Havinson, I. V. Khatuntsev, A. V. Kiselev, L. V. Ksanfomality, Yu. V. Nikolsky, P. Masson, O. Forni, and C. Sotin, Topography of the Martian tropical regions with ISM, *Planetary Science Letters, 39*, 1/2 , 225-236, 1991.

Bibring, J. P., Global and high resolution surface mineralogical mapping OMEGA/Mars Express, In *Concepts and approaches for Mars exploration*, Lunar and Planetary Institute, 26 pages, 2000.

Christensen, P. R., D. L. Anderson, S. C. Chase, R. N. Clark, H. H. Kieffer, M. C. Malin, J. C. Pearl, J. Carpenter, N. Bandiera, F. G. Brown, and S. Silverman, Thermal Emission Spectrometer experiment: Mars Observer mission, *J. of Geophys. Res., 97*, 7719-7734, 1992.

Christensen, P. R., and H. J. Moore, The Martian surface layer, In *Mars*, 686-729, 1992.

Christensen, P. R., G. L. Mehall, N. Gorelick, and S. Silverman, The Athena miniature thermal spectrometer (Mini-TES), In *Concepts and approaches for Mars exploration*, 67-68, 2000.

Christensen, P. R., J. L. Bandfield, V. E. Hamilton, D. A. Howard, M. D. Lane, J. L. Piatek, S. W. Ruff, and W. L. Stefanov, A thermal emission spectral library of rock-forming minerals, *J. Geophys. Res., 105,* 9735-9739, 2000.

Christensen, P. R., J. L. Bandfield, V. E. Hamilton, S. W. Ruff, H. H. Kieffer, T. N. Titus, M. C. Malin, R. V. Morris, M. D. Lane, R. L. Clark, B. M. Jakosky, M. T. Mellon, J. C. Pearl, B. J. Conrath, M. D. Smith, R. T. Clancy, R. O. Kuzmin, T. Roush, G. L. Mehall, N. Gorelick, K. Bender, K. Murray, S. Dason, E. Greene, S. Silverman, and M. Greenfield, Mars Global Surveyor Thermal Emission Spectrometer experiment: Investigation description and surface science results, *J. of Geophys. Res., 106*, 23823-23871, 2001a.

Christensen, P. R., R. V. Morris, M. D. Lane, J. L. Bandfield, and M. C. Malin, Global mapping of Martian hematite mineral deposits: Remnants of water-driven processes on early Mars, *J. of Geophys. Res., 106*, 23,873-23,885, 2001b.

Christensen, P. R., B. M. Jakosky, H. H. Kieffer, M. C. Malin, H. Y. McSween, Jr., K. Nealson, G. L. Mehall, S. H. Silverman, S. Ferry, M. Caplinger, The Thermal Emission Imaging System (THEMIS) for the Mars 2001 Odyssey mission, *JGR, submitted*, 2002.

Combes, M., C. Car, P. Drossart, T. Encrenaz, E. Lellouch, J. Rosenqvist, J. P. Bibring, S. Erard, B. Gondet, Y. Langevin, A. Soufflot, V. I. Moroz, A. V. Grygoriev, L. V. Ksanfomality, Yu. V. Nikolsky, N. F. Sanko, and D. V. Titov, Martian atmosphere studies from the ISM experiment, *Planetary Space Science, 39*, 1/2, 189-197, 1991.

Coskren, D. and W.H. Blackburn, Equilibration between aluminous pyroxene and plagioclase; A geobarometer-geothermometer, *Eos, 53*, 549, 1972.

Conrath, B., R. Curren, R. Hanel, V. Kunde, W. Maguire, J. Pearl, J. Pirraglia, and J. Walker, Atmospheric and surface properties of Mars obtained by infrared spectroscopy on Mariner 9, *J. Geophys. Res., 78*, 4267-4278, 1973.

Dollfus, A., and Deschamps, M. Grain-size determination at the surface of Mars, *Icarus, 67*, 37-50, 1986.

Feely, K. C., and P. R. Christensen, Quantitative compositional analysis using thermal emission spectroscopy: Application to igneous and metamorphic rocks, *J. of Geophys. Res., 102*, 25593-25603, 1997.

Folco, L., and I. A. Franchi, Dar Al Gani 670 shergottite: A new fragment of the Dar Al Gani 476/489 Martian meteorite, In *63rd Annual Meteoritical Society Meeting*, Abstract #5209, Meteoritical Society of America, 2000.

Hamilton, V. E., Determination of Martian meteorite lithologies and mineralogies using vibrational spectroscopy, J. Geophys. Res., 102, 25,593-25,603, 1997.

Hamilton, V. E., The effect of particle size on rock spectra in the thermal infrared: Implications for TES data analysis, In *Lunar and Planetary Science XXX*, Abstract #2001, Lunar and Planetary Institute, Houston, CD-ROM, 1999.

Hamilton, V. E., and P. R. Christensen, Determining the modal mineralogy of mafic and ultramafic igneous rocks using thermal emission spectroscopy, *J. Geophys. Res., 105,* 9717-9734, 2000.

Hamilton, V. E., M. B. Wyatt, H. Y. McSween Jr., and P. R. Christensen, Analysis of terrestrial and Martian volcanic compositions using thermal emission spectroscopy: II. Application to Martian surface spectra from the Mars Global Surveyor Thermal Emission Spectrometer, *J. Geophys. Res., 106,* 14,733-14,746, 2001a.

Hamilton, V. E., H.Y. McSween, Jr., and P. R. Christensen, Searching for Martian meteorite source regions using Mars Global Surveyor, Thermal Emission Spectrometer (MGS TES) data, In 64th Meteoritical Society Meeting, Abstract #5128, 2001b.

Hamilton, V. E., P. R. Christensen, and H. Y. McSween, Jr., Global constraints on Martian meteorite source regions: Deconvolutions of MGS TES data using SNC meteorites as end members, In *Lunar and Planetary Science XXXIII*, Abstract #1937, Lunar and Planetary Institute, Houston, CD-ROM, 2002.

Hanel, R. A., B. J. Conrath, W. A. Hovis, V. G. Kunde, P. D. Lowman, J. C. Pearl, C. Prabhakara, and B. Schlachman, Infrared spectroscopy experiment on the Mariner 9 mission; Preliminary results, *Science, 175*, 305-308, 1972a.

Hanel, R. A., B. J. Conrath, W. A. Hovis, V. G. Kunde, P. D. Lowman, J. C. Pearl, C. Prabhakara, B. Schlachman, G. Levin, and T. E. Burke, Overview of results from the infrared spectroscopy experiment on Mariner 9, *American Astronomical Society of Planetary Sciences Annual Meeting Abstracts, 2*, 6, 1972b.

Hanel, R. A., B. J. Conrath, W. A. Hovis, V. G. Kunde, P. D. Lowman, J. C. Pearl, C. Prabhakara, and B. Schlachman, Infrared Spectroscopy Experiment on the Mariner 9 mission: Preliminary results, *Science, 175*, 305-308, 1972c.

Hanel, R., Results from the Infrared Spectroscopy Experiment on Mariner 9, *COSPAR Plenary Meetings Program and Abstracts, 16*, 208, 1973c.

Hardie, L. A., Origin of $CaCl_2$ brines by basalt-seawater interaction: Insights provided by some simple mass balance calculations, *Contributions to Mineralogy & Petrology, 82*, 2-3, 205-213, 1983.

Head, L., and J.W. Head III, Cryomagmatism, processes of generation, ascent and eruption and application to Europa, In *Lunar and Planetary Science XXX*, Abstract #1689, Lunar and Planetary Institute (CD-ROM), 1999.

Ikeda, Y. H. Takeda, M. Kimura, and A. Suzuki, A new shergottite from Oman, Dhofar 378, In *Lunar and Planetary Science XXXIII*, Abstract #1434, Lunar and Planetary Institute, Houston (CD-ROM), 2002.

Imae, N., R. Okazaki, H. Kojima, and K. Nagao, The first nakhlite from Antarctica, In *Lunar and Planetary Science XXX111*, Abstract #1483, Lunar and Planetary Institute, Houston (CD-ROM), 2002.

Kahle, A. B., A. R. Gillespie, E. A. Abbott, M. J. Abrams, R. E. Walker, and G. Hoover, Relative dating of Hawaiian lava flows using multispectral thermal infrared images: A new tool for geologic mapping of young volcanic terranes, *J. of Geophysical Research, 93*, 15239-15251, 1988.

Kahle, A. B., F. D. Palluconi, and P. R. Christensen, Thermal emission spectroscopy: Application to the Earth and Mars, *In Remote Geochemical Analysis: Elemental and Mineralogical Composition (ed. by Pieters and Englert)*, 99-120, 1997.

Kieffer, H. H., S. C. Chase, Jr., E. Miner, G. Muench, and G. Neugebauer, Preliminary report on infrared radiometric measurements from the Mariner 9 spacecraft, *J. of Geophys. Research, 78*, 4291-4312, 1973.

Kieffer, H. H., Soil and surface temperatures at the Viking landing sites, *Science, 194*, 1344-1346, 1976.

Kieffer, H. H., S. C. Chase, Jr., E. D. Miner, F. D. Palluconi, G. Munch, G. Neugebauer, and T. Z. Martin, Infrared thermal mapping of the Martian surface and atmosphere: First results, *Science, 193*, 780-785, 1976.

Kieffer, H. H., P. R. Christensen, T. Z. Martin, E. D. Miner, and F. D. Palluconi, Temperatures of the Martian surface and atmosphere: Viking observation of diurnal and geometric variations, *Science, 194*, 1976.

Kinzler, R. J., J. M. Donnelly-Nolan, and T. L. Grove, Late Holocene hydrous mafic magmatism at the Paint Pot Crater and Callahan flows, Medicine Lake Volcano, N.

California and the influence of H (sub 2), In the generation of silicic magmas, *Contributions to Mineralogy and Petrology, 138*, 1-16, 2000.

Kozlowski, R. W., A. L. Sprague, and L. A. Lebofsky, Comparison of thermal emission spectra from the surfaces of Mercury and the Moon, *Lunar and Planetary Science XX*, Abstracts, 540-541, 1989.

Ksanfomaility, L. I., and V. I. Moroz,, *Kosmicheskiye Issledovaniya, 13*, 1, 1-128, 1975.

Lin, C. Y., F.S., Zhang, H. N. Wang, R. C. Wang, and W. L. Zhang, Antarctic GRV9927: A new member of SNC meteorites, In *Lunar and Planetary Science XXXIII*, Abstract #1562, Lunar and Planetary Institute, Houston (CD-ROM), 2002.

Livingstone, W. A., Voyager infrared observations of the outer solar system, PhD dissertation, 140 pages, Cornell University, 1990.

Logan, L. M., and G. R. Hunt, Emission spectra of particulate silicates under simulated lunar conditions, *J. of Geophys. Res., 75*, 6539-6548, 1970.

Lopes-Gautier-Rosaly, M. C., A. G. Davies, R. W. Carlson, W. D. Smythe, L. W. Kamp, L. A. Soderblom, F. E. Leader, and R. Mehlman, Hot spots on Io; initial results from Galileo's near infrared mapping spectrometer, *Geophysical Research Letters, 24*, 2439-2442, 1997.

Lucey, P. G., Comparison of thermal emission spectroscopic measurements of the lunar surface; 1968-1990, In *Proceedings of Lunar and Planetary Science* XXI, 417-423, 1991.

Lunine, J. I., Sulfur lakes and silicate flows; thermal emission from Io's hot spots, In Time-variable phenomena in the Jovian system, *NASA Special Publication*, 63-70, 1989.

Lyon, R. J. P., W. M. Tuddenham, and C. S. Thompson, Quantitative mineralogy in 30 minutes, *Economic Geology, 54*, 1047-1055, 1959.

Lyon, R. J. P., Evaluation of infrared spectroscopy for compositional analysis of lunar and planetary soils, final report, contract NASr, 49(04), Stanford Research Institute, Menlo Park, CA, 1962.

Lyon R. J. P., and E. A. Burns, Analysis of rock and minerals by reflected infrared radiation, *Economic Geology, 58*, 274-284, 1963

Lyon, R. J. P., Analysis of rocks by spectral infrared emission (8 to 25 microns), *Economic Geology, 60*, 715-736, 1965.

Mansor, S. B., A. P. Cracknell, B. V. Shilin, and V. I. Gornyi, Monitoring of underground coal fires using thermal infrared data, *International Journal of Remote Sensing, 15*, 1675-1685, 1994.

McSween, H. Y., Jr., and A. H. Treiman, Martian meteorites, In *Reviews in Mineralogy Vol. 36: Planetary Materials* (ed. by J. J. Papike), Mineralogical Society of America, 1998.

McSween, H. Y., Jr., Basalt or andesite? A critical evaluation of constraints on the composition of the ancient Martian crust, In *Lunar and Planetary Science XXXIII*, Abstract #1062, Lunar and Planetary Institute, Houston (CD-ROM) 2002.

Mikouchi, T. and M. Miyamoto, Olivine cooling rate of the northwest Africa 1068 Shergottite, In *Lunar and Planetary Science XXXIII*, Abstract #1346, Lunar and Planetary Institute, Houston (CD-ROM), 2002.

Miner, E. and T. Gombosi, Cassini Saturn Orbiter science investigations, Cassini mission to Saturn, http://www.jpl.nasa.gov/cassini/Science/orbiter.html., 2000.

Moersch, J. E., and P. R. Christensen, Thermal emission from particulate surfaces: A comparison of scattering models with measured spectra, *J. Geophys. Res.*, *100*, 7465-7477, 1995.

Mustard, J. F., and J. E. Hays, Effects of hyperfine particles on reflectance spectra from 0.3 to 25 μm, *Icarus*, *125*, 145-163, 1997.

Nakamura, T., A. M. Nakamura, J. Saito, S. Sasaki, R. Nakamura, D. Hirohide, H. Akiyama, and D. Tholen, Multi-band imaging camera and its sciences for the Japanese near-Earth asteroid mission MUSES-C, *Earth, Planets and Space, 53*, 11, 1047-1063, 2001.

Nash, W. P., Plagioclase resorption phenomena and geobarometry in basic lavas, *EOS, 57,* 507, 1973.

Nelson, R. M., W. D. Smythe, B. D. Wallis, L. J. Horn, A. L. Lane, and M. J. Mayo, Temperature and thermal emissivity of the surface of Neptune's satellite Triton, *Science*, *250*, 429-431, 1990.

Neugebauer, G., G. Munch, H. Kieffer, J. S. C. Chase, and E. Miner, Mariner 1969 infrared radiometer results: Temperatures and thermal properties of the Martian surface, *Astron. J., 76,* 719-728, 1971.

Norrish, K., and J. T. Hutton, An accurate x-ray spectrographic method for the analysis of a wide range of geological samples, *Geochimica et Cosmochimica Acta, 33*, 431-453, 1969.

Oppenheimer, C., P. W. Francis, D. A. Rothery, R. W. T. Carlton, and L. S. Glaze, Infrared image analysis of volcanic thermal features; Lascar Volcano, Chile, 1984-1992, *J. of Geophys. Res.*, *98*, 4269-4286, 1993.

Papike, J. J., Comparative planetary mineralogy: Chemistry of melt-derived pyroxene, feldspar, and olivine, In *Reviews in Mineralogy Vol. 36: Planetary Materials* (ed. by J. J. Papike), Mineralogical Society of America, 1998. -

Ramsey, M. S., and P. R. Christensen, Mineral abundance determination: Quantitative deconvolution of thermal emission spectra, *J. of Geophys. Res.*, *103*, 579-596, 1998.

Rosenbauer, R. J., J. L., Bischoff, and R. A. Zierenberg, The laboratory albitization of mid-ocean ridge basalt, *Journal of Geology, 96*, 237-244, 1988.

Rubin, A. E., P. H. Warren, J. P. Greenwood, R. S. Verish, L. A. Leshin, and R. L. Hervig, Petrology of Los Angeles: A new basaltic shergottite find, In *Lunar and Planetary Science XXXI*, Abstract #1963, Lunar and Planetary Institute, Houston (CD-ROM), 2000.

Ruff, S. W., P. R. Christensen, P. W. Barbera, and D. L. Anderson, Quantitative thermal emission spectroscopy of minerals: A laboratory technique for measurement and calibration, *J. Geophys. Res., 102*, 14,899-14,913, 1997.

Ruff, S. W., Quantitative thermal infrared emission spectroscopy applied to granitoid petrology, PhD dissertation, 234 pages, Arizona State University, 1998.

Salisbury, J. W. and J. W. Eastes, The effect of parcel size and porosity of spectral contrast in the mid-infrared, *Icarus*, *64*, 586-588, 1985.

Salisbury, J. W., and A. Wald, The role of volume scattering in reducing spectral contrast of restrahlen bands in spectra of powdered minerals, *Icarus, 96*, 121-128, 1992.

Smith, M. D., J. L. Bandfield, and P. R. Christensen, Separation of atmospheric and surface spectral features in mars Global Surveyor Thermal Emission Spectrometer (TES) spectra: models and atmospheric properties, *J. Geophys. Res., 105*, 9589-9608, 2000.

Sinton, W. M. On the composition of Martian surface materials, *Icarus*, 6, 222-228, 1967.

Sinton, W. M., and J. Strong, Radiometry of Mars, *Astrophysical Journal, 131*, 459-469, 1956.

Shorthill, R. W., H. J. Moore, R. F. Scott, R. E. Hutton, S. Liebes, Jr., and C. R. Spitzer, The "soil" of Mars (Viking 1), *Science, 194*, 91-97, 1976.

Snyder, C. W., and V. I. Moroz, Spacecraft exploration of Mars, In *Mars* (ed. by H. H. Kieffer, B.M. Jakosky, C.W. Snyder, and M.S. Matthews), Univ. of Arizona Press, 1992.

Soffen, G. A., Scientific results of the Viking missions, *Science, 194*, 1274-1276, 1976.

Stakes, D. S., and P. Schiffman, hydrothermal alteration within the basement of the sedimented ridge environment of Middle Valley, northern Juan de Fuca Ridge, *GSA Bulletin, 3*, 9, 1294-1314, 1999.

Taylor, L. A., A. Patchen, D. H. S. Taylor, J. G. Chambers, and D. S. McKay, X-ray digital imaging and petrography of lunar mare soils: Data input for remote sensing applications, *Icarus*, *124*, 500-512, 1996.

Taylor, L. A., M. A. Nazarov, M. A. Ivanova, A. Patchen, R. N. Clayton, and T. K. Mayeda, Petrology of the Dhofar 019 shergottite, In *Abstracts from the 63rd Annual Meteoritical Society Meeting*, Abstract #5047, Meteoritical Society of America, 2000.

Thomson, J. L., and J. W. Salisbury, The mid-infrared reflectance of mineral mixtures (7-14mm), *Remote Sensing of the Environment*, *45*, 1-13, 1993.

Tyler, A. L., R. W. Kozlowski, and L. A. Lebofsky, Determination of rock type on Mercury and the Moon through remote sensing in the thermal infrared, *Geophysical Research Letters, 15*, 808-811, 1988.

Van Tassel, R. A. and J. W. Salisbury, The composition of the Martian surface, *Icarus*, 3, 264-269, 1964.

Wanke, H., and G. Dreibus, Chemical composition and accretion history of terrestrial planets, *Phil Trns. R. Soc. Lond. A325*, 545-557, 1988.

Watson, K. C. and L. C. Rowan, Recent application of thermal infrared data for mineral exploration and environmental studies, SEG Annual Meeting Tech. Program Abs. With Biographies, 66, 1150-1152, 1996.

Whyte, F., Dumbarton Rock, *Scottish Journal of Geology, 2*, 107-121, 1966.

Wyatt, M. B., and H. Y. McSween, Jr., An alternative hypothesis for basalt and andesite on Mars: Global surface compositions from MGS-TES, In *Meteoritical Society 64th Annual Meeting*, Abstract #5392, 2001.

Wyatt, M. B., V. E. Hamilton, H.Y. McSween, Jr., P. R. Christensen, and L. A. Taylor, Analysis of terrestrial and Martian volcanic compositions using thermal emission spectroscopy: 1. Determination of mineralogy, chemistry, and classification strategies, *J. Geophys. Res.*, *106*, 14711-14732, 2001.

Wyatt, M. B., and H. Y. McSween, Jr., Andesite or weathered basalt? Martian surface compositions from MGS-TES, In *Lunar and Planetary Science XXXIII*, Abstract #1702, Lunar and Planetary Institute, Houston (CD-ROM) 2002.

Wyatt, M. B., and H. Y. McSween, Jr., Spectral evidence for weathered basalt as an alternative to andesite in the northern lowlands of Mars, *Nature*, *417*, 263-266, 2002.

Yanai, K., New Martian meteorite identified as a lherzolitic shergottite similar to ALH-77005 meteorite, In *Lunar and Planetary Science XXXIII*, Abstract #1248, Lunar and Planetary Institute, Houston (CD-ROM), 2002.

Zheng, L., Z. Zuji, and C. Lin, Practice and research on short-term earthquake prediction by interpreting satellite thermal infrared anomaly image, *Earth Science*, *21*, 665-668, 1996.

Zipfel, J., B Spettel, H. Palme, and G. Dreibus, Petrology and chemistry of Dar Al Gani 476, a new basaltic shergottite, In *Lunar and Planetary Science XXX*, Abstract #1206, Lunar and Planetary Institute, Houston (CD-ROM), 1999.

Zipfel, J., Sayh Al Uhaymir 005/008 and its relationship to DAG 476/489, In *Abstracts from the 63rd Annual Meteoritical Society Meeting*, Abstract #5147, Meteoritical Society of America, 2000.

APPENDICES

See attached CD-ROM (plate 1) for Appendix material

The CD contains Appendices A-H that can be accessed by inserting the CD into the CD-ROM drive and opening the CD via the file manager. Appendix files are in either Microsoft Word or Microsoft Excel format

Vita

Keith A. Milam was born on December 28, 1974, in Bowling Green, Kentucky. From an early age, he had an avid interest in space exploration and had a lifelong goal of becoming an astronaut. His academic interests were scientific in nature and upon his graduation from Warren Central High School, he enrolled at Western Kentucky University. Keith majored in geology with an emphasis in karst hydrology, but his senior research projects focused on impact cratering, involving the Barringer Meteor Crater and Middlesboro impact structures.

After two years of working as staff geologist for the American Cave Museum in Horse Cave, Kentucky, and as a park ranger at Mammoth Cave National Park, Keith enrolled in the master's degree program in the Department of Geological Sciences at the University of Tennessee in Knoxville. There his research focused on laboratory verification of martian remote sensing techniques, while doing impact-cratering research as a side hobby. Keith is currently pursuing a doctorate in geology at the University of Tennessee.